1964

Solar Cycle Effects on Inner Belt Protons

Robert C. Blanchard
College of William & Mary - Arts & Sciences

SOLAR CYCLE EFFECTS ON INNER BELT PROTONS

A Thesis

Presented to

The faculty of the Department of Physics

The College of William and Mary in Virginia

In Partial Fulfillment

of the Requirements for the Degree of

Master of Arts

by

R. C. Blanchard

June, 1964

APPROVAL SHEET

This thesis is submitted in partial fulfillment of
the requirement for the degree of
Master of Arts

Robert C. Blanchard
Author

Approved, June, 1964:

James D. Lawrence, Jr., Ph.D.

Donald E. McLennan

Robert E. Welsh

Frederic R. Crownfield, Jr.

Wilmot N. Hess

TABLE OF CONTENTS

LIST OF FIGURES

LIST OF TABLES

ABSTRACT

This report presents a study of the solar cycle variation of the proton population of the inner radiation belt. The analysis includes proton energies from 10 to 700 Mev. An appropriate field line, L = 1.25, and various values of field strength, B, are investigated. A particle conservation equation containing sources and losses of inner belt protons is established using an averaged atmosphere and numerically integrated over a number of solar cycles. The proton source term used in the conservation equation is the atmosphere decaying albedo neutrons, while the loss processes used are atmospheric ionization and nuclear interactions. Using Harris and Priester's (3) models, an averaged atmospheric model is constructed in terms of B, L coordinates which represents the number density trapped particles would, on the average, encounter. The process includes diurnal, longitudinal, north-south and "bounce" averaging. The time dependence of the model is constructed for a typical solar cycle using averaged information of the recent past. Although the model is time dependent, it is independent of a particular solar cycle. Both steady-state and transient conditions are calculated as a function of belt coordinates. Proton flux spectra for solar maximum and solar minimum are calculated. Transient spectra are presented showing the dynamical behavior of trapped protons when influenced by the fluctuating atmosphere. Comparisons

are made with the transient and steady-state proton population calculations. The results indicate that the proton population is changed by an order of magnitude from solar maximum to solar minimum for low energy protons, E < 100 Mev. Higher energy protons, E > 300 Mev are not appreciably effected. Mean proton lifetimes are calculated as a function of energy and B at solar minimum and solar maximum.

SOLAR CYCLE EFFECTS ON INNER BELT PROTONS

INTRODUCTION

The discovery of the earth's radiation belt by the Explorer I flight of May, 1958 (Van Allen, Ludwig, Ray, McIlwain) has initiated much interest in trapped particle phenomena. In the following five years, data has been collected and analyzed, yielding a great deal of piecemeal information describing the radiation belts. The complexity of the problem, along with the unusual, but necessary, equipment, that is, satellites, has hidden the complete explanation of trapped particles. The inner zone of the radiation belt, defined as altitudes less than approximately one earth radii, has been more thoroughly investigated. This is probably due to its proximity and the state-of-the-art of booster and tracking abilities at the time of the belt discovery. Contributions of researchers dealing with the exploration of the inner belt are reviewed as background for the more recent publication by Pizzella[2] which initiated this investigation.

Before Van Allen's discovery, research was progessing along another path; that of explaining the polar aurora caused by charged particles. In 1903, Störmer studied the motion of a charged particle in a dipole field in an attempt to explain auroral phenomena. A dipole field was used since this model represents the earth's field to a first approximation. He found that charged particles coming from infinity could not be trapped by a dipole field like the earth.

The particles would either strike the earth, or be deflected by the magnetic field and return to infinity. Consequently, workers in the field were led to the conclusion that the inner regions were empty of extra-terrestrial particles. Störmer's work on the study of motion of charged particles in the vicinity of a dipole field proved a valuable stepping-stone in light of the belt discoveries 55 years later.

An important advance, as far as earth trapped particles are concerned, came 50 years later. In 1953 Treiman's calculations of cosmic ray secondaries, or "albedo" particles, to explain rocket measurements indicated that low energy particles could exist in the earth's magnetic field. The idea of the albedo particle hypothesis came to be one of the more accepted sources in recent years for high energy protons in the inner belt. The current albedo hypothesis is as follows: extra-terrestrial particles strike the atmosphere producing neutrons and other particles. The neutrons, not being affected by the earth's magnetic field, scatter in all directions. After a short time (i.e. 10^3 seconds) the neutrons decay into protons. The resulting protons are affected by the earth's magnetic field such that some are "trapped", that is, confined to a region above the earth's surface. If the altitude at which the trapping occurs is low, the protons will be readily lost by collisions with the atmosphere and will not significantly contribute to the belt population. When, however, the trapping occurs above the dense lower atmosphere, the protons will stay longer and thus contribute significantly to the belt population. This breakthrough stimulated new interest in explaining the aurora by trapped charged particles. Singer (1955) postulated the existence of trapped particles to produce an earth bound ring current. Singer used the perturbation theory of trapped charged particles formulated by Alfven (1950), which predicts that charged particles will drift in longitude and thereby produce an effective longitudinal current. The interaction of the ring current and the magnetic field was investigated analytically. An unsuccessful attempt was made in November, 1957 to substantiate Singer's work. A half year later, two U. S. satellites, 1958α and 1958γ, (Explorers I and III) carrying Geiger counters showed anomalous counting rates at an altitude of approximately one earth radii. Van Allen's correct interpretation of the Geiger counter readings as due to high flux encounters of trapped particles opened new paths in the exploration and description of the trapped particle phenomena.

A description of the belt usually involves the following six quantities:

(1) J_i - the omnidirectional flux of the type particle, i having energy E (where i = proton, electron, etc.)

(2) (r, λ, θ) - the coordinates of the point under consideration.

(3) E - the kinetic energy of the i particle.

(4) t - time

By utilizing the geomagnetic coordinates, L and B, the spatial dependence can be greatly simplified. The use of this coordinate system is essentially due to the fact that trapped particles possess a longitudinal adiabatic constant of motion, I, which can be utilized in mapping. The fact that particles are "trapped," that is, the magnetic moment μ of a charged particle is a constant of the motion (see Appendix B for discussion) produces a "mirroring" motion whereby a particle spirals about a field line between a magnetic field B_o in the northern hemisphere and the same value B_o in the southern hemisphere. Due to inhomogeneities in the field, the whole configuration drifts. The drift is such that

$$I = \oint_{M}^{M'} \sqrt{1 - \frac{B}{B_o}}\, d\ell$$

is a constant. I is called the longitudinal integral invariant and M and M' are the northern and southern mirror points and B_o is the value of the field at M. The locus of B and I produces rings in the northern and southern hemisphere where the southern rings are called the conjugate rings. The locii of lines of force connecting the rings are defined as a magnetic shell. Thus, rather than describing measurements of flux at points in space by r, λ, and θ, the spatial distribution of trapped particles is defined by

---

There are actually three adiabatic constants of motion of trapped particles. These are the magnetic moment, the longitudinal invariant and the flux invariant. These constants are usually called adiabatic since their constancy depends upon how rapidly the magnetic field changes.

labeling the magnetic shells by B_o, and I since the particle flux is approximately constant on this shell[10]. McIlwain [10] in 1961 introduced a parameter, L, where L = f (I, B) to label the magnetic shells. The parameter L is more conceptually convenient since for a dipole field, it is equal to the equatorial distance from the center of the earth to the line of force. At present, the use of the "natural" coordinates B and L is an accepted system by researchers involved in the exploration of the trapped particles.

Soon after Van Allen's discovery, satellites fitted with counters were sent to obtain data on the trapped particles. Two satellites were sent in the middle of 1958 to explore the spatial distributions of the new phenomena. They were Explorer IV (Van Allen, McIlwain, Ludwig, 1959) and Sputnik III (Vernov and Chudakov, 1960). The data from both satellites indicated two distinct regions of high particle flux with a low particle flux at L = 2 e.r. Pioneer III, a space probe carrying geiger counters and launched in December, 1958, indicated the same result. The two regions were called the inner and outer radiation zones, while the in-between region with the low counting rate was called the "slot." As subsequent satellites were sent with more discriminating particle counters, the idea of two distinct regions became less believable. Explorer XII (O'Brian, Laughlin, 1962) data indicated that the whole region is occupied with low energy electrons ($E \geq 40$ Kev) and protons ($E \geq 100$ Kev) with approximately the same intensities. It is now believed that the earlier satellites which were equipped with non-discriminating counters, probably encountered the high energy protons at $L < 2$ e.r., and the high energy electrons at $L > 2$ e.r., thus producing the two distinct regions. The names, Inner and Outer region, have been kept by researchers for historical reasons and also to indicate two possible origins.

A current description of the radiation belt is given by Figure I-1. (This has been reproduced with the permission of Hess[26]). The figure describes the radiation belt by separating the omnidirectional flux of protons and electrons into energy categories. The omnidirectional flux for the different energy categories are plotted in R, λ space where R is the geocentric distance and λ is the magnetic latitude. That is, the magnetic coordinates B and L are transformed to R and λ through the dipole field equations (these are stated in Appendix A). It can be seen from the two lower figures of high energy protons and electrons why the early experimenters, who used non-discriminating counters, might have distinguished the belt into two regions. An excellent review of the discoveries leading to the current spatial description of the radiation belt is given in References 26, 27 and 28. The protons which are investigated in this study are the higher energy protons, statically described by the lower right-hand figure. The portion of space considered in this study, as can be seen from this figure, is confined roughly to magnetic latitudes of 30° and geocentric distances of 1.2 to 2.0 earth radii. The protons are probably the best established component of the radiation belt, mainly due to data taken by Freden and White from nuclear emulsion stacks flown in April, 1959 and October, 1960.

Soon after data became available, trapped particle researchers began to verify their theories of mechanisms describing the radiation belt. A model evolved containing two processes; a source and a loss process of trapped protons. The source of the inner belt protons was found to be reflected atmospheric decaying neutrons coming from galactic cosmic ray collisions, while the loss of protons was found to be due to near atmospheric collisions. Investigators[7,9,16,17,18] have established these mechanisms from data. A brief review of their contributions will be made in order to establish the model used in this study. Utilization of their contributions will be made throughout, whenever possible.

Papers by Lenchek and Singer[16,17] Freden and White[7,18], Hess[9] have shown good comparisons with the data using reflected atmospheric neutrons due to galactic cosmic rays as a source for inner belt protons. The data in the comparisons were taken from the nuclear emulsion stack flown on April, 1959 and October, 1960. (Freden and White). The energy spectrum of the source used to evaluate the data was found to be a function of E^{-2}. There is some small difference as to the power of E according to Singer[16]. This difference is 0.2 and, for the most part, would not appreciably affect the results. Furthermore, it is pointed out by Singer that this is within the observational accuracy of the data. In accordance, the source spectrum of protons in this paper will be $f(E^{-2})$.

Removal processes for protons trapped in the belt have been investigated by various people[1,7,9,16,17,18]. Lenchek and Singer's[17] paper enumerates the current theories for proton losses. They are, elastic or Coulomb scattering, inelastic scattering, nuclear interactions, and losses due to non-adiabatic effects. The inelastic scattering, referred to as the ionization loss mechanism by others, is a significant contributing factor to proton losses throughout most of the energies considered in the paper, becoming dominant at lower energies $E < 300$ Mev. This loss mechanism is used in describing the proton population. Elastic scattering, although of major importance to light trapped particles like electrons, is considered to be negligible for the heavy particles, like protons[17]. Consequently, elastic scattering is not considered. The nuclear interaction losses, that is, proton losses due to catastrophic destruction by running into atmospheric constituents, thereby causing a nuclear reaction, have been used by Freden and White[7] and Lenchek and Singer[17] in their analysis of proton fluxes for high energy protons ($E > 300$ Mev). They indicate that the inclusion of this loss process becomes necessary at higher energies[17,7]. Since this energy range is of interest, this mechanism is used along with elastic scattering. The last loss mechanism, non-adiabatic effects, is discussed by Lenchek and Singer[17]. The criteria of this condition is,

$$\left|\frac{\nabla B}{B}\right| << \frac{1}{a}$$

That is, the magnetic field doesn't change appreciably as the particle spirals about a field line with a radius equal to a. To obtain a rough idea of the size of this condition, consider a 700 Mev proton near the equator spiraling around the L = 1.25 line. The ratio of B/∇B for a dipole field approximation is

$$\frac{B}{\nabla B} = \frac{r}{3} \approx 3 \times 10^{8} \text{ cm}$$

The radius of gyration, which near the equator is the largest, of a 700 Mev proton mirroring at large latitudes is:

$$a = \frac{mv}{q}\sqrt{\frac{1}{B_e B_m}} = \frac{1.7(10^{-24})\,2.5(10^{10})}{1.6(10^{-20})}\sqrt{\frac{1}{(.15)(.26)}}$$

$a = 2 \times 10^{7}$ cm

Or, a is smaller than B/∇B. As the velocity decreases the radius of gyration decreases and the adiabatic condition is less apt to break down. Thus, the loss of protons due to the breakdown of the adiabatic condition will not be considered.

To summarize, of the four removal theories mentioned, only inelastic scattering and nuclear interactions are used in this paper. The remaining two are omitted for the following reasons respectively; 1) the trapped charged particles investigated are protons; 2) the energies of the protons are > 10 Mev; 3) the lines of force are confined to the inner region of the radiation belt. Or, referring to Figure I-1, the protion of the belt investigated as a function of time is described by the lower right hand figure which can be adequately calculated by using a cosmic ray albedo source and the aforementioned loss processes.

Previous observations have not indicated large variations in the proton population of the inner part of the radiation belt.

Outer belt ($L > 2$) measurements, on the other hand, have shown large variations and are currently being studied. Pizzella[2] indicated in his paper that Yoshida, Ludwig and Van Allen (1960) have shown from Explorer I data that the change in the proton population is less than a factor of 2 for a two month period. Data from Explorer IV (McIlwain, 1961) indicated the same results for a three month period. However, Pizzella's[2] collected data from the Explorer VII satellite for a period of fourteen months definitely indicates a trend in a sizeable change of the inner belt population. The plots of counting rate versus time (for $L = 1.25$ to 1.5) presented by Pizzella[2](Fig. 4) show a steady increase in counting rate with some superimposed variations. Although the net change is about 4 or 5 ($L = 1.5$) to 2 or 3 ($L = 1.25$) for the fourteen month period, there is a steady increase in the belt population. This leads to curious questions: why the steady increase -- and what will be its net change? An attempt is made in this paper to answer these questions by investigating the effects that the expanding and collapsing atmosphere in conjunction with a time varying source have on the trapped protons in the inner belt. The solar cycle dependence of the intensity of galactic cosmic rays has been investigated by McDonald and Webber[20,19]. A current estimate[19] of the relative change of neutron solar source strength from solar maximum to solar minimum is 25%, where solar maximum is smaller due to the exclusion of some galactic particles by the Sun's increased activity. In addition to the change in source strength is the periodic change of the atmosphere density by approximately an order of magnitude due to exospheric heating[3]. It turns out that these two effects are resonant. That is, at solar minimum, the atmosphere is less dense and collisions are less on the average, thereby allowing the protons to live longer. At the same time, the source strength is a maximum, or more protons on the average are being supplied into the belt due to the decreased activity of the sun. Thus, the net effect is that more protons are available at solar minimum as compared to solar maximum where the opposite effect takes place. It is believed that these two factors should produce a noticeable effect over a period of time equal to a solar cycle (approximately 11 years). It is also believed that some of the steady change in counting rate observed from data taken over a short period of time (as compared to the duration of a typical solar cycle) collected by Pizzella could be due to this effect. A study has been completed which investigates these effects on the proton population using current available information. The method by which the problem is attacked, and the results of the study are presented in the following sections.

ANALYSIS AND CALCULATIONS

The Average Atmospheric Models

The study of the proton population depends primarily on the atmosphere since losses of protons are due to the atmosphere. The atmosphere is a function of many variables, like latitude, time of day, height, etc. To develop the atmosphere in a detailed manner considering all the variables would be difficult. However, it is possible to construct an average model which, over long sampling periods, would give a reasonable representation of the earth's atmosphere. This is by no means anything new. However, an attempt will be made in this section to develop a solar cycle time dependent atmosphere in terms of what a trapped particle would "see" while moving about the Earth's magnetic field. (See Appendix B for discussion of trapped particle motion The averaged models will be transformed into B, L space since this choice of coordinates has been adapted by most trapped particle experimenters. The B, L transformation used is that developed by McIlwain[10] using the 48 spherical harmonic coefficients of Jenson and Cain[11]. This transformation has been programmed for a 7090 IBM digital computer. The input to the program is the geocentric spherical coordinates (h, λ, ϕ), where h is altitude in km, λ is geocentric latitude in degrees, and ϕ is geocentric longitude in degrees. Basically the program numerically integrates the longitudinal invariant I using a series expansion for the magnetic field. Then using a dipole representation of the earth, the program calculates L which is a function of I and B. This program is currently being used at the Goddard Space Flight Center Theoretical Division[12].

The basic models used in this study are the ones generated by Harris and Priester[3] which give the hourly number density for five atmospheric constituents, N_2, O_2, H_e, H, O. There are five models generated. Each model refers to a given solar radiation flux in units of 10^{-22} watts/m^2/cycle/sec. The link between solar flux, S and time is given by Figure 1. (This has been reproduced with the permission of Harris and Priester[3]). The dotted line superimposed on the curve represents the average yearly variation of S with time. Notice that the cycle is unsymmetrical. This unsymmetrical nature of the time variation will appear later in the proton population calculation. As seen from the curve, the S variation begins at 1947. Since the results are applied to recent data and since an estimate of the flux for the coming solar minimum is of interest, an approximate extrapolation has been made. The extrapolation beyond 1961 is an average between the extrapolation of Figure 1 and corresponding values less than January, 1954. The constructed mean solar cycle with epoch at January, 1954, is given by Figure 2. As can be seen, the unsymmetrical nature is retained. It must be noted here that this curve represents an estimate for the next four years using information from the current solar cycle and assuming the cycle will last 11 years.

The first step in arriving at the average models is to calculate the diurnal average number density of each of the five models presented by Harris and Priester[3]. The sum,

$$\bar{n}^j = \frac{1}{24} \sum_{i=1}^{24} n_i^j \quad \text{atoms/cm}^3$$

is computed where the five atmospheric elements are $j = H_e$, O, O_2, N_2, H and where i refers to the hourly value of the density. The values of $\bar{n}^j$ are presented in tabular form as a function of S and altitude in Tables 1 through 5. The diurnal average is taken because protons drifting in longitude around the earth have periods of revolution on the order of 1 to 30 minutes[9]. Thus, over a period of 24 hours the daily proton population variation will tend to be averaged out, or at least be a second order effect compared to the solar cycle expansion of the atmosphere, which is 11 years. This does not mean that the longitudinal drift of trapped protons is being neglected, but that the short term time effects will not be considered.

The second step in constructing the solar cycle average atmosphere is to consider the longitudinal drift of protons along a B, L contour. Contours of northern and southern field lines were generated using the B, L digital code[10,11,12] previously mentioned. Figures 3 and 4 show the B contours for L = 1.25 as a function of altitude and longitude. Figure 4 represents the southern conjugate field lines of Figure 3. Both figures show the inhomogeneity of the earth's field in the northern and southern hemisphere. As is seen by comparison of these two figures, the southern hemisphere minimum altitude is lower by approximately 600 or 700 km than the northern lines near longitude -40°. This is what is commonly referred to as the South Atlantic anomaly. The maximum altitude for a given B, L contour occurs in the northern hemisphere. For this particular L line the maximum altitude is not appreciably greater in the northern hemisphere than in the southern hemisphere. The calculation of the longitudinal average density $\bar{\bar{n}}_k^j$ is done by the sum

$$\bar{\bar{n}}_K^j = \frac{1}{35} \sum_{i=1}^{36} \bar{n}_i^j(\varphi) \quad \text{atoms/cm}^3$$

where k refers to northern or southern hemisphere and where $\bar{n}_i^j(\varphi)$ is the diurnal average number density of the jth constituent at longitude φ which corresponds to an altitude from figures 3 and 4. The factor 35 is used because equal increments of 10° in longitude were used to evaluate $\bar{\bar{n}}_k^j$. The longitudinal average was performed for both southern and northern hemispheres for each of the five S models and for each of the five constituents. Both hemispheres were then averaged together to give a composite longitudinal average $\bar{\bar{n}}^j$ of the jth atmosphere constituent. As might be suspected, the composite longitude model is strongly influenced by the southern anomaly which dips low in altitude. Extrapolation was necessary since the atmospheric tables (Tables 1 through 5) used in calculating the longitudinal average include altitudes of $120 \leq h \leq 2000$ km. The range of extrapolation can be seen from figures 5 and 6. These figures are constant minimum altitudes in the southern hemisphere and constant maximum altitudes in the northern hemisphere cross-plotted into B, L space. These figures were reproduced with the permission of Hess, Blanchard, Stassinopoulos[13] From figures 5 and 6 the limit of the tables for L = 1.25 lies between B's of .231 and .168 where the maximum altitude is obtained from the northern hemisphere and the minimum altitude is from the southern hemisphere. Values of density above and below these B's were obtained by logarithmic extrapolation.

The last averaging step is to adjust $\bar{\bar{n}}^j$ due to the protons north-south mirroring motion. This process, in essence, reduces the magnitude of the tables due to the motion of a proton from a mirror point at low altitude and high density moving towards the equator at a high altitude and low density. As one might expect, the amount by which $\bar{\bar{n}}^j$ is reduced depends upon the arc distance away from the equator. As the arc distance approaches zero, the correction factor becomes one. The calculation of the "bounce" average $\bar{\bar{\bar{n}}}^j$ is made by evaluating the integral; (See Appendix A for derivation and discussion of the bounce average)

$$\bar{\bar{\bar{n}}}^j = \frac{\int_0^{\lambda_0} A(\lambda)\,\bar{\bar{n}}^j(\lambda)\,d\lambda}{\int_0^{\lambda_0} A(\lambda)\,d\lambda} \qquad \text{atoms/cm}^3$$

where

$$A(\lambda) = \cos^4\lambda \left[\frac{4 - 3\cos^2\lambda}{a\cos^6\lambda - b\sqrt{4 - 3\cos^2\lambda}}\right]^{1/2}$$

$$a = \sqrt{4 - 3\cos^2\lambda_0}$$

$$b = \cos^6\lambda_0$$

λ_o = mirror point latitude

$\bar{\bar{n}}^j(\lambda)$ = longitudinal atmospheric number density of the jth constituent as a function of latitude, λ.

The integral is evaluated numerically for the five S models and the five atmospheric constituents. The $\bar{\bar{n}}^j$ (B) tables were transformed into $\bar{\bar{n}}^j$ (λ) by the magnetic dipole transform

$$B = \frac{M(1 + 3\sin^2\lambda)^{1/2}}{r_e^3 L^3 \cos^6\lambda}$$

The A (λ) is introduced into the integral due to the fact that protons are spiraling about the field line, rather than bouncing back and forth along the field line. The spiraling motion is such that protons stay longer near the mirror point than at the equator. This effect is taken into account by weighing the average calculation with respect to latitude, by the inclusion of A (λ).

Upon completion of the bounce average, the atmosphere constituents are now constructed in terms of what the trapped particles would encounter. The functional dependence is solar flux S, magnetic induction B, and field line L = 1.25. The 5 constituents are put together to form the average number of oxygen atoms/cm^3 by

$$\bar{\bar{\bar{\rho}}} = 1.75\,\bar{\bar{\bar{n}}}^{(N_2)} + \bar{\bar{\bar{n}}}^{(O)} + .25\,\bar{\bar{\bar{n}}}^{(He)} + 2\,\bar{\bar{\bar{n}}}^{(O_2)} + .125\,\bar{\bar{\bar{n}}}^{(H)}$$

for each of the 5 S models. The atmosphere is represented in terms of oxygen in order to relate the energy loss due to the atmosphere with data taken by Aron, Hoffman and Williams[5]. This procedure of representing the atmosphere in terms of the average oxygen number density will become more apparent in Section B where the particle conservation equation components are described. Figure 7 shows $\overset{\equiv}{\rho}$ as a function of B for the 5 S models at L = 1.25.

As is seen from this figure, the S models meet at about B = .25. That is, the model corresponding to solar maximum (S = 250) is the same as the model at solar minimum (S = 70). This effect indicates that near B's of this value for L = 1.25 the solar cycle effect is negligible.

The models generated are for a particular line of force, L = 1.25 and the 5 S models. From Figure 2, S versus time, it is a straight forward calculation to eliminate S for time by interpolating between the curves. Figure 8 shows the resulting time dependence of the atmosphere in terms of the scale factor,

$$\underline{R}(L=1.25, B, t) = \frac{(\text{oxygen atoms/cm}^3)_{ATMOS}}{(\text{oxygen atoms/cm}^3)_{NTP}}$$

where $(\text{oxygen atoms/cm}^3)_{NTP}$ comes from the following relationship of an ideal gas:

$$22414 \text{ cm}^3/\text{kmole} = .60249 \times 10^{24} \text{ atoms/kmole}$$

or

$$(\text{oxygen atoms/cm}^3)_{NTP} = 2.69 \times 10^{19}$$

The ratio R is calculated in order to relate the energy loss of the atmosphere with the measured energy loss data[5]. Explicitly, the energy loss/unit length at NTP conditions for an oxygen absorber is given in Reference 5. To find the corresponding energy loss/length for the atmospheric conditions which is represented in terms of oxygen, one multiplies by R.

The net result in constructing the atmosphere in the preceding fashion is mainly to eliminate directional difficulties in the following discussion of proton spectra and lifetimes. As can be seen from each of the averaging processes an attempt has been made to represent the atmosphere in terms of what the trapped particle would encounter while moving about the earth or, in other words, replacing the problem by an averaged time dependent absorber which varies periodically with a period of 11 years.

The Particle Conservation Equation

The study of the variation in the proton population requires knowledge of the conditions which governs how protons are supplied to a given region and what processes take protons out of the same region. In other words, what are the sources and sinks for trapped particles? If they were known completely, a particle conservation could be established and the proton population would be known at any instant of time and position. It is attempted in this section to describe the proton population on an average basis using the decaying atmospheric neutrons as the source of protons and to develop the solar cycle average ionization and nuclear interaction losses. The purpose of this section is to construct the particle conservation equation used in the study. The resultant equation will be similar to that used by Freden and White[7], Lenchek and Singer[17] and Hess[1,9] in their studies of neutrons as a source and the steady-state proton population.

The continuity equation can be written as

$$\frac{\partial N}{\partial t} + \nabla \cdot \bar{J} = 0 \tag{1}$$

where $\frac{\partial N}{\partial t}$ is the time change in the number of particles/cm^3 at a given point. This is a statement of the conservation of particles which does not involve any sources or sinks, that is, particles being created or destroyed inside the volume. Equation (1) also stipulates that the particles can be described by specifying the spatial coordinates only. That is, at a given time the particles in the volume are not distinguishable. As was stated earlier, it is convenient to describe the trapped particles at any time by distinguishing the particles by their energies since a given particle may change its energy. To introduce the concept that the particles being counted are described by both position and energy, it is necessary to write equation (1) in four dimensional space, with E as the fourth dimension. That is,

$$\frac{\partial N}{\partial t} + \nabla_4 \cdot \bar{J} = 0 \qquad (2)$$

where

$$N = N(x, y, z, E, t)$$

$$\nabla_4 = \left(\frac{\partial}{\partial x}, \frac{\partial}{\partial y}, \frac{\partial}{\partial z}, \frac{\partial}{\partial E} \right)$$

$$\bar{J} = \left(J_x, J_y, J_z, J_E \right) = N \left(\frac{\partial x}{\partial t}, \frac{\partial y}{\partial t}, \frac{\partial z}{\partial t}, \frac{\partial E}{\partial t} \right)$$

Considering the trapped particles to be protons and separating out the 4th component, equation (2) can be written as,

$$\frac{\partial N_p}{\partial t} + \nabla_x \cdot \bar{J} + \frac{\partial J_E}{\partial E} = 0 \qquad (3)$$

Where,

N_p = proton number density (protons/cm^3-Mev)

$\bar{v}$ = proton velocity ($\dot{x}$, $\dot{y}$, $\dot{z}$) (cm/sec)

$\bar{J}$ = $N_p\bar{v}$, proton flux density (protons/cm^2-Mev-sec)

∇_x = spatial gradient ($\frac{\partial}{\partial x}, \frac{\partial}{\partial y}, \frac{\partial}{\partial z}$)

E = kinetic energy of the protons under investigation (Mev)

J_E = $N_p \frac{\partial E}{\partial t}$, energy component of the flux density

Equation (3) represents the conservation of particles which have energy E. That is, the divergence term accounts for particles leaving a volume while the extra term in equation (3) accounts for the change in the proton density due to the changes in proton energy inside the volume.

The assumption is made that

$$\nabla_x \cdot \bar{J} = 0$$

That is, the region under investigation is such that the flux inside is a constant with respect to position. The element of volume considered is a tubular shaped cylinder centered about a line of force, L, extending from a fixed magnetic field B_o in the northern hemisphere to the same value in the southern hemisphere. The change in proton number of protons of energy E would be due to gains or losses of energy inside the volume. With this in mind, equation (3) becomes

$$\frac{\partial N_p}{\partial t} + \frac{\partial}{\partial E}\left(N_p \frac{\partial E}{\partial t} \right) = 0 \qquad (4)$$

Protons of energy E are being added to the volume due to decaying albedo neutrons and, similarily, protons at energy E are being lost by catastrophic collisions with other particles. To account for these phenomena, equation (4) is adjusted to,

$$\frac{\partial N_p}{\partial t} + \frac{\partial}{\partial E}\left(N_p \frac{\partial E}{\partial t}\right) = S - L_N$$

Rearranging leaves:

$$\frac{\partial N_p}{\partial t} = S - L_N - \frac{\partial}{\partial E}\left(N_p \frac{\partial E}{\partial t}\right) \qquad (5)$$

where the change of the proton population with respect to time at a given energy E is given as three terms; a source of protons S, a loss of protons L_N, and a change of energy of the protons due to atmospheric absorption of energy. In other words, a field line L is chosen and a mirror magnetic induction B_O is fixed. The change in the average number density of protons at time t, of energy E, at B_O, L is of interest. Protons of energy E gyrating from northern to southern mirror points run into atoms of the atmosphere and are destroyed and no longer available for counting, this is the L_N term. Protons of energy E are being supplied into the field line by decaying albedo neutrons, and consequently are available for counting; this is the S term. Finally, protons of energy E lose some of their energy by ionizing the atmospheric atoms and consequently are not counted since they are of different energy. This effect is included in the last term in Equation (5). Thus, equation (5) represents the conservation condition of trapped protons which yields the rate of change of the proton number density with time, while the integral gives the total number of protons/cm^3 - Mev, or the proton population at any time t.

As stated earlier, to describe the proton population it is necessary to include all sources and losses. However, as discussed previously, it is possible to omit some. This can be done by limiting the region of applicability of the results. With this in mind, the two terms S and L_N will be expanded into a convenient form.

The nuclear interaction loss term L_N used in this study is basically that used by Freden and White[7]. Let $\sigma(j)$ be the area of the jth atom of the atmosphere such that if a proton hits that area it will be destroyed. $\bar{\bar{\bar{n}}}^j$ is the average number of j atoms/cm^3 available in the volume. If J is the incident flux, then the fraction of flux loss in passing through a volume of thickness dl is:

$$\frac{\Delta J}{J} = \bar{\bar{\bar{n}}}^j \sigma(j)\, dl$$

The loss rate of the number of protons/cm^3 in terms of flux is

$$L_N = \frac{1}{v} \frac{\Delta J}{\Delta t}$$

From the above equation of the fraction of flux loss by passing through the element of volume, the L_N term becomes

$$L_N = \frac{1}{v} J \bar{\bar{\bar{n}}}^j \sigma(j) \frac{\Delta l}{\Delta t}$$

Or,

$$L_N = N_p v \sum_{j=1}^{5} \bar{\bar{\bar{n}}}^j \sigma(j) \qquad (6)$$

where $\bar{\bar{\bar{n}}}^j$ is the average number of j atoms/cm^3 of the jth constituent of the atmosphere previously calculated and $\sigma(j)$ is the interaction cross section of the jth constituent and the 5 indicates the number of constituents considered.

By defining

$$\Sigma = \sum_{j=1}^{5} \bar{\bar{\bar{n}}}^{j} \sigma(j)$$

equation (6) can be written more conveniently as

$$L_N = N_p v \Sigma$$

The value of σ for oxygen used for the calculation of Σ is from Freden and White[7] which is

$$\sigma(O) = .36 \times 10^{-24} \ \text{cm}^2$$

The interaction cross section of Helium used is

$$\sigma(He) = .143 \times 10^{-24} \ \text{cm}^2$$

For simplicity of calculation, it is assumed that the Nitrogen interaction cross section is equal to that of Oxygen and the Hydrogen contribution is negligible. Thus, the calculation of Σ is,

$$\Sigma = \frac{\bar{\bar{\bar{n}}}^{(He)}}{2} \sigma(He) + \left[\frac{\bar{\bar{\bar{n}}}^{(O)} + 2\bar{\bar{\bar{n}}}^{(O_2)}}{8} + \frac{2\bar{\bar{\bar{n}}}^{(N_2)}}{7} \right] \sigma(O) \quad \text{atoms/cm}$$

The pulsation of the atmosphere causes the Σ to be a function of time in the solar cycle as well as position. Figure 9 shows $\log_e \Sigma$ as a function of time for various values of B at L = 1.25. It can be seen that as B increases, the variation from solar maximum to solar minimum decreases. Or, as might be suspected, the "breathing" atmosphere is not as pronounced at large B's which corresponds to low altitudes.

The source of protons, as was stated earlier, came from resulting albedo neutron decays. The neutrons are produced from cosmic ray protons colliding with oxygen and nitrogen. The produced neutron scatter in all directions and subsequently decayed into protons. The neutrons which escape from the atmosphere and subsequently decay will be injected into the belt. The form of the proton source, S to be used in this study is essentially the same as that used by Hess[1] with some minor modifications. Specifically, these are the addition of the solar cycle time dependence and the transformation into B,L space. Due to the nearly equal masses of protons and neutrons the energy of the proton resulting from neutron decay is very near the energy of the parent neutron. It is possible to assume that the proton's energy, and direction of motion is that of the parent neutron; or that the source of protons is equal to the decay density of neutrons. That is,

$$S(E) \approx \frac{dn(E)}{dV} \qquad \text{neutrons/cm}^3\text{-sec-Mev}$$

where

$dn(E)$ is the number of decaying neutrons/sec at energy E (neutrons/sec/Mev)

dV is the element of volume (cm^3)

If n is the number of undecayed neutrons present in an element of volume dV and the average life of the neutrons before decaying into protons is τ seconds, then the number of decaying neutrons per unit time is

$$dn = \frac{n}{\tau}$$

Letting N be the number of neutrons/cm^3 in the element of volume gives

$$dn = \frac{N\,dV}{\tau}$$

Or, the number of decaying neutrons/sec/element of volume is

$$\frac{dn}{dV} = \frac{N}{\tau}$$

Defining J_N as the neutron flux results in the source of protons as

$$S = \frac{dn}{dV} = \frac{J_N}{v\tau}$$

The neutron flux leaking out of the atmosphere has been calculated[26] from measurements of the neutron energy spectrum inside the atmosphere. The resultant flux of these neutrons, in the energy range considered in this study, was found to be

$$J_N = .8E^{-2} f(r) \qquad \text{neutrons/cm}^2\text{-sec-Mev}$$

where f(r) is a non-dimensional spatial dependence of the neutron flux. Following Hess[1], the decay density of neutrons is given approximately by

$$S = \frac{dn}{dV} = \frac{\varphi}{v\gamma\tau}\left(\frac{r_e}{r}\right)^2 \exp\left[-\frac{r}{v\gamma\tau}\right]$$

where r_e is the equatorial radius of the earth ($r_e = 6378.2\times10^5$ cm.) and where γ has been added to account for the dilated neutron mean life. The other quantities in this equation are defined as follows:

v = neutron velocity (cm/sec)

β = v/c

γ = $(1 - \beta^2)^{-\frac{1}{2}}$

c = speed of light, 2.9979×10^{10} cm/sec

τ = neutron mean life, 10^3 sec

r_e = radius of earth, 6378.2×10^5 cm

φ = calculated equatorial neutron flux and is given by $.8E^{-2}$ neutrons/cm^2-Mev-sec.

It is already assumed that the velocity of the parent neutron is the same as the velocity of the decayed proton. In the preceding calculations, the evaluation of v, β and γ in S will be done by considering only protons.

For the region of consideration of this study, the exponential factor is approximately equal to 1. For example, the distance from the center of the earth to the line L = 1.25 is $\sim 10^9$ cm, and the slowest speed of neutrons considered is $v \sim 4\times10^9$ cm/sec, which is roughly 10 Mev. Thus, the value of the exponential is:

$$\exp\left[\frac{-r}{v\gamma\tau}\right] = \exp\left[\frac{-10^9}{4(10^9)(1.1)10^3}\right] \approx 1.0$$

The result of the simplification leaves the source term as,

$$S = \frac{dn}{dV} = \frac{\varphi}{\beta c\gamma\tau}\left(\frac{r_e}{r}\right)^2$$

A modification of the neutron leakage, φ, is made using information obtained from McDonald[19]. The value used by Hess[1] of φ is

$$\varphi = .8E^{-2}$$

where φ is not a function of time. A non-dimensional parameter Φ, is defined as the relative inner belt source strength. That is,

$$\Phi(t) = \frac{\varphi(t,E)}{\varphi(t_o,E)} = \frac{K(t)E^{-2}}{.8E^{-2}} = \frac{K(t)}{.8}$$

Figure 10 shows $\Phi(t)$ as a function of time for the recent past. Again, the non-symmetrical nature of the current solar cycle becomes apparent from this figure. As seen from this figure, the relative change from solar maximum to solar minimum is 25% where solar maximum is the smaller due to the exclusion of galactic particles, which produce the neutrons, by the increased activity of the sun. This out-of-phase of the source and loss process helps contribute in a positive way to the net change of the proton population between solar maximum and solar minimum. That is, at solar minimum, the loss process, or basically the atmosphere, is small compared to solar maximum. This means that protons are not taken out as rapidly. On top of this, the source is pumping in protons at its maximum rate. These two effects act together to give a net change of more protons at solar minimum. However, as can be seen from this figure and figure 7, the atmosphere has a much larger effect then the variable source.

One modification of σ results in changing equation (7) to

$$S = \frac{.8\,\Phi(t)\,E^{-2}}{\beta c \gamma \tau}\left(\frac{r_e}{r}\right)^2 \qquad (8)$$

The second modification is to change the position variables to B, L space. This is done by using a dipole earth approximation[15].

$$B = \frac{M(4 - 3\cos^2\lambda)^{1/2}}{r_e^3 L^3 \cos^6\lambda} \tag{9}$$

and

$$\frac{r}{r_e} = L\cos^2\lambda$$

where M is the earth's dipole moment (8.1×10^{25} gauss. cm^3).

That leaves equation (8) as

$$S = \frac{.8\,\Phi(t)\,E^{-2}}{\beta c \gamma \tau L^2 \cos^4\lambda} \tag{10}$$

where the λ dependence is replaced by B through equation (9). The $\cos^{-4}\lambda$ term is left in the equation due to inability of equation (9) to be solved in closed form.

For the calculations, it is assumed that the source term S produces protons from decaying neutrons such that all produced protons have velocity orientations perpendicular to the field, B at a given latitude, λ_o. That is, all protons produced are injected at the mirror latitude, λ_o. This assumption is made instead of adding the contributions of protons at other positions along a field line which have the necessary mirror point conditions (that is, the proper pitch angle, α where α is the angle between $\bar{B}$ and the velocity of the proton $\bar{v}$). Or, the injection coefficient used is 1. This assumption would probably not affect the general result of the study which is relative change from solar minimum to solar maximum.

Equations (6) and (10) represent the form of the components of equation (5) to be numerically integrated. Before substituting S and L_N into equation (5) there is some rearranging which can be done in order to set up the equation for numerical integration. Expanding equation (5), gives

$$\frac{\partial N_p}{\partial t} = S - \frac{\partial N_p}{\partial E}\frac{\partial E}{\partial t} - N_p \frac{\partial}{\partial E}\left(\frac{\partial E}{\partial t}\right) - L_N = S - \frac{\partial N_p}{\partial t} - N_p \frac{\partial}{\partial E}\left(\frac{\partial E}{\partial t}\right) - L_N$$

rearranging results in

$$\frac{\partial N_p}{\partial t} = \frac{S}{2} - \frac{N_p}{2}\frac{\partial}{\partial E}\left(\frac{\partial E}{\partial t}\right) - \frac{L_N}{2} \qquad (11)$$

expanding by the chain rule

$$\frac{dE}{dt} = \frac{dE}{dx}\frac{dx}{dt} = \beta c \frac{dE}{dx}$$

where, as before $\beta = v/c$ and v = proton velocity (cm/sec) and c = speed of light. Substituting into equation (11) and expanding results in

$$\frac{dN_p}{dt} = \frac{S}{2} - \frac{N_p c}{2}\left[\frac{d\beta}{dE}\frac{dE}{dx} + \beta\frac{d}{dE}\left(\frac{dE}{dx}\right)\right] - \frac{L_N}{2} \qquad (12)$$

From Freden and White[7], the values of β and γ are given in terms of E in two regions of the energy spectra. The values are for $10 \leq E < 80$ Mev.

$$\beta = .0484\ E^{.477}$$

$$\gamma = .930\ E^{.022}$$

for $80 \leq E \leq 700$ Mev (13)

$$\beta = .0896\ E^{.344}$$

$$\nu = .428\ E^{.205}$$

Notice that the curve fit to the two separate energy regions does not come together at E = 80 Mev. This approximation is overcome by smoothing the resulting spectra in this region. By taking the derivatives of β with respect to E, gives

$$\frac{d\beta}{dE} = .0231\ E^{-.523} \qquad \text{for} \quad 10 \leq E < 80 \text{ Mev}$$

(14)

$$\frac{d\beta}{dE} = .0308\ E^{-.656} \qquad \text{for} \quad 80 \leq E < 700 \text{ Mev}$$

Substituting equations (6), (10), (13), (14) into equation (12) and performing the multiplication, the particle conservation equation becomes

$$\frac{dN_p}{dt} = \frac{A_0 \Phi}{L^2 E^{B_0} \cos^4 \lambda_0} - \frac{A_1 N_p}{E^{B_1}}\left(\frac{dE}{dx}\right) - A_2 N_p E^{B_2} \frac{d}{dE}\left(\frac{dE}{dx}\right) - A_2 E^{B_2} N_p \Sigma \qquad (15)$$

where, if the energy is $10 \leq E < 80$ Mev

$A_0 = 2.694 \times 10^{-13}$ $\qquad B_0 = 2.509$

$A_1 = 3.463 \times 10^{8}$ $\qquad B_1 = .523$

$A_2 = 7.255 \times 10^{8}$ $\qquad B_2 = .477$

and if the energy is $80 \leq E \leq 700$ Mev

$A_0 = 3.479 \times 10^{-13}$ $\qquad B_0 = 2.549$

$A_1 = 4.617 \times 10^{8}$ $\qquad B_1 = .656$

$A_2 = 1.343 \times 10^{9}$ $\qquad B_2 = .344$

Equation (15) is the form of the particle conservation equation used for the study of the proton population as a function of time. The equation is numerically integrated using a fixed step, first-order Runge Kutta technique[21]. That is, the equation written symbolically as

$$\frac{dN_p}{dt} = f(N_p, E, L, B, t)$$

is solved by first choosing L = 1.25, a value B, and energy E. Then choosing an integration interval Δt and initial conditions t_o, and N_{po}, the integration is as follows: calculate

$$\Delta N_p = \tfrac{1}{6}(K_1 + 2K_2 + 3K_3 + K_4)$$

where

$$K_1 = f(N_{po}, t_o)\Delta t$$
$$K_2 = f(N_{po} + K_1/2, t_o + \Delta t/2)\Delta t$$
$$K_3 = f(N_{po} + K_2/2, t_o + \Delta t/2)\Delta t$$
$$K_4 = f(N_{po} + K_3, t_o + \Delta t)\Delta t$$

The first step answer becomes $N_{p_1} = N_{po} + \Delta N_p$. The above calculation continues using the time $t_1 = t_o + \Delta t$. Control of the error is handled by appropriately adjusting the integrating interval Δt. As can be seen from the integrating technique outlined, the function $f(N_p, E, L\ B_o, t)$ needs to be evaluated at different times for a given E, L, B_o. The quantities to be supplied are

$$\frac{dE}{dx}, \quad \frac{d}{dE}\left(\frac{dE}{dx}\right), \quad \Phi, \quad \Sigma$$

The energy loss term $\frac{dE}{dx}$ is calculated as a function of E, B, L time. Figure 11 shows the energy loss versus energy for an oxygen absorber at NTP conditions. The curve comes from data published by Aron, Hoffman, and Williams[5]. As was stated earlier in the construction of the model atmospheres, in order to relate the energy loss of the atmosphere with the measured data, the R function (figure 8) is used. Or, to look at it in another way, for a given energy E the scale number is found from figure 11. With this value, the curves of figure 8 are adjusted by multiplying by the scale number. In this fashion, the energy loss, $\frac{dE}{dx}$ term becomes a function of B, L, and time. Physically, this term represents the energy given per path length to the atmospheric atoms by the protons.

From figure 11 the slope is calculated to produce $\frac{d}{dE}(dE/dx)$ as a function of energy E. Figure 12 shows the results of the calculation. The calculation of $\frac{d}{dE}(dE/dx)$ as a function of E, B, L, and t is done in the same fashion as $\frac{dE}{dx}$. That is, for a given energy E, the scale number of $\frac{d}{dE}(dE/dx)$ is found and the curves of figure 8 adjusted appropriately. This term represents the rate of energy loss of the trapped protons.

The values of σ and ϕ are given by figures 9 and 10 respectively. As can be seen, ϕ, the relative source strength is given only as a function of time, the reason being that both the position and energy dependence have been factored out of ϕ in the development of the source term. The "effective cross-section," σ, is a function of time and position, where the energy dependence has been retained in the rest of the nuclear interaction term.

A difficulty arises when evaluating the transient proton number density. As can be seen from equation (15) an initial value for N_p is necessary in order to integrate the equation. If one assumes initially that there are no protons (i.e., $N_{pi} = 0$) at time t_o, then an assumption is needed as to whether to inject protons into the belt at solar maximum, at solar minimum, or sometime in between. For the study of the transient spectrum with $N_{pi} = 0$, it is assumed that protons are injected at solar minimum. This is done to investigate the most rapid build-up since at solar minimum, the injection of protons is the largest while the removal process is the smallest.

Following the work done earlier,(7, 17, 9) the steady-state proton population is found by setting

$$\frac{dN_p}{dt} = 0$$

that is, assuming the net rate of change of the proton number density is small. Equation (15) then becomes

$$N_p = \frac{A_o \Phi}{L^2 E^{B_o}\left[\frac{A_1}{E^{B_1}}\frac{dE}{dx} + A_2 E^{B_2}\frac{d}{dE}\left(\frac{dE}{dx}\right) + A_2 E^{B_2}\sum\right]\cos^4\lambda_o} \qquad (16)$$

where the coefficients are those defined previously.

As can be seen from the functional dependence of $N_p = N_p(E, B_o, L, t)$, a time must be chosen in order to evaluate the steady-state spectrum for a given position. Two times are chosen, solar maximum and solar minimum. This is done in order to investigate the maximum change in proton number density at the two source and loss extremes.

RESULTS AND CONCLUSIONS

The calculation of the proton population of the inner belt $L = 1.25$, as a function of the soler cycle has indicated that;

(a). The transient time of buildup of protons to steady-state conditions increases as B decreases. As the proton energy decreases the time necessary to build the radiation belt decreases.

(b). Protons with energies > 300 Mev are not extremely effected by the fluctuating atmosphere.

(c). Protons with energies $25 \leq E < 300$ show a relative change in population of less than an order of magnitude, while extremely low energies, $E < 25$ Mev, indicate a two order magnitude change in population.

(d). The transient steady-state conditions indicate that for low energy protons ($E < 25$ Mev), the transient proton flux is less than the steady-state flux at solar minimum and the same at solar maximum. The amount of reduction is a function of B, whereas B decreases, the reduction is increased.

(e). Time histories of the proton population indicate that due to the "ability" of low energy protons ($E \lesssim 25$ Mev) to follow the breathing atmosphere, while higher energy protons do not, there is a change in the nature of the energy spectrum of the population where the spectrum becomes peaked near energy 100 Mev. This change occurs for a relatively abrupt atmosphere change, such as the change from solar minimum to solar maximum used in this study; Figure 2.

(f). At solar minimum, protons at low B live longer by a factor of $\sim 10^2$ than at solar maximum. As B increases, the factor is reduced to less than 10.

These conclusions are based on the results found from evaluating equations (15) and (16). The evaluation was done on an IBM 7090 digital computer. The results from these equations are presented on Figure 13 to 16.

Figures 13 and 14 are plots of proton flux versus proton energy for L = 1.25 and B's equal to .199 and .209 gauss respectively. The dotted line of each of these graphs represents the solution of equation (16) for solar minimum and solar maximum with

$$\frac{dN_p}{dt} = 0$$

That is, the steady-state solution. The solid lines represent the steady-state flux found from equation (15) starting with $N_{pi} = 0$ and t_i = solar minimum. The steady-state proton flux is found by letting the source and loss mechanisms operate until the belt is saturated. The saturation test is that two corresponding cycles become numerically identical. To digress on this, Figure 15 indicates the time required in terms of solar cycles (11 years) to build the steady-state conditions. As can be seen, at high energies and small B, the buildup takes hundreds of years; Conclusion (a). It is interesting to note the different buildup times as a function of B, which is incremented in 0.1 gauss. For energy > 300 Mev the change in time for an increment of .1 gauss for B > .2 is almost twice that for the same increment at B < .18. Below B = .219 the buildup is difficult to detect due to the extremely low flux and the almost non-existent variation in the atmosphere.

The proton flux at the two extremes under the above steady-state conditions are plotted in Figures 13 and 14. These spectrums show conclusions (b), (c), and (d). Notice the small variation of the solid curve between solar maximum and solar minimum for the two curves at energies > 300 Mev. In this area of the spectrum, the same result could have been obtained by including one more step in the averaging calculation, that is, by averaging Figure 2. The corresponding averaged solar cycle atmosphere could be utilized in the steady-state solution, equation (16), to find the proton population. As seen from Figure 15, this would eliminate a great deal of numerical calculations.

From Figures 13 and 14 at E < 300 Mev, the dynamical behavior of the atmosphere becomes more predominant. The lower solid line (solar maximum) approaches the steady-state solution more rapidly than the upper solid line (solar minimum). As B increases, the effect happens at higher energies. It is believed that this phenomena is a direct result of the unsymmetrical cycle variation of the atmosphere. Examining Figure 2, it is seen that from solar minimum to solar maximum the change is abrupt, the time taking approximately twice as long. This uneven fluctuation causes the low energy protons to "follow" or be in phase with the changing atmosphere for the lower solid curve (solar maximum) and not "follow" the fluctuating atmosphere at solar minimum; Conclusion (d). As might be expected, the calculation of the lower energy protons could have been done by using the steady-state equation with the atmospheric model corresponding to the time in the solar cycle. Observing figure 13 indicates that the results would be more in agreement at solar maximum than at solar minimum. The range of energy where the simplification in calculation is applicable would depend on the shape of the cycle.

The relative change in magnitude of flux at solar cycle extremes in the lower energy part of the spectrums is indicated on figures 13 and 14; Conclusion (c). As is seen from these figures the change of proton flux from solar minimum to solar maximum is nearly two orders of magnitude near E ~ 10 Mev, and decreases as energy increases.

Figure 16 shows the time history of proton flux for two cycles, the first and the tenth, at different energies. This graph indicates Conclusion (c). That is, low energy protons due to their "ability" to follow the changes of the atmosphere show marked variations throughout the solar cycle. High energy protons, on the other hand, are not extremely affected by the fluctuating atmosphere. This effect causes a change in the spectra where protons of high energy become predominant. The shape of the cycle will influence at what energy the shifting occurs, that is, if the cycle variation used was less abrupt, it is expected that the 25 Mev curve would not cross the 100 Mev curve, but perhaps some lower energy. Conclusion (e) is again seen in this Figure. Notice how rapidly the 25 Mev protons build up on the first cycle as compared with the tenth cycle, while the 500 Mev protons are slowly building up to the tenth cycle.

Following Hess[1] and others, the mean lifetimes of protons are calculated. That is, the average lifetime t is calculated from information obtained by equation (16) by the "leaking bucket" equation, which is;

$$t = \frac{\text{contents}}{\text{input}} = \frac{N_p}{S}$$

Figures 17 and 18 are plots of proton lifetimes versus energy for increments of B = .1 gauss at L = 1.25 for the two source and loss extremes. Conclusion (f) is based on these graphs. It is interesting to note the spacing between the curves. For solar maximum, increments of B of .1 gauss indicate an almost constant amount of adjustment to the proton lifetime. While the same increment for solar minimum shows an order of magnitude difference in lifetime for B > .2 when compared to B < .18. This sort of effect was seen on the discussion of Figure 15. This might be explained by two effects. First, for a given line, the collapsing atmosphere allows the protons to live longer, since the atmospheric loss is smaller. This is a shifting of the ordinate between the solar maximum and solar minimum curves. The second effect is that when the atmosphere collapses due to a lesser amount of exospheric heating, the "edge" of the sensible atmosphere is shifted to lower altitudes. This shifting of the "edge" would account for the spread of the curves at solar minimum since some values of B lie above the sensible atmosphere.

To summarize, indications are that the time fluctuations of the atmosphere play an important role in the proton population of the inner belt. Calculations indicate that there is a substantial change in the inner belt population due to solar cycle atmospheric effects. Also, along with the relative change of protons in the cycle, there is a change in the nature of the proton energy spectra. It is expected that this change is dependent on the shape of the cycle and the time within the cycle. The steady increase of count rate seen in the data collected by Pizzella[2] for $L < 1.5$ could have been the effect of the current cycle which is approaching solar minimum. Data extending over a much longer period of time than available today is needed in order to substantiate a great deal of the conclusions. The reason being that the atmosphere is constructed such that it averages out short-time effects. It is believed by the author that such a collection of data would be fruitful insofar as that it would bring out a great deal of interesting phenomena about trapped particles and solidify the state-of-the-art source and loss mechanisms of inner belt protons.

Appendix A

This appendix will discuss the method used in the fourth step in the development of the average atmospheric models. As was discussed, there is a need to adjust the tables due to the motion of trapped particles spiraling about a field line going from northern mirror point to southern mirror point encountering different densities. This motion is shown pictorially by Figure A-I. The method will assume a dipole earth. The procedure will be to find the average density encountered by the particles' north-south spiraling motion, referred to as the "bounce" motion, in terms of latitude for a given field line, L.

Following Ray[6], the bounce average of the number density is defined as;

$$\bar{\rho} = \frac{\int \rho(B,L)\, ds}{\int ds} \qquad (1)$$

That is, the bounce average, $\bar{\rho}$ for a given mirror point, λ_0 and field line, L is the average number of atoms/cm^3 that a particle "sees" while spiraling about a field line from the northern to southern mirror points (Figure A-I). Since the earth is assumed to be a dipole, the magnetic field is symmetrical about the magnetic equator. Due to symmetry, the integral need only be evaluated over 1/4 of a complete oscillation. The procedure adopted for the calculation of equation (1) is to project the element of arc ds onto the field line, L. This is done for convenience since the atmosphere is given in terms of field lines.

The element of arc ds = v dt where v is the particles' total velocity along the helical path. The component parallel to the field line is $V_{\parallel} = V \cos \alpha$ where α is the "pitch" angle, or the angle between the field vector $\bar{B}$ and the vector $\bar{V}$

$$ds = \frac{V_{\parallel}\, dt}{\cos\alpha} = \frac{d\ell}{\cos\alpha}$$

Substituting into equation (1).

$$\bar{\rho} = \frac{\int \rho(B,L)\, d\ell / \cos\alpha}{\int d\ell / \cos\alpha} \tag{2}$$

To find $d\ell$ in terms of latitude, consider an element of arc in polar coordinates (r, λ).

$$d\ell = \sqrt{dr^2 + r^2 d\lambda^2} = \sqrt{\left(\frac{dr}{d\lambda}\right)^2 + r^2}\; d\lambda \tag{3}$$

using the differential of the equation of a field line for a dipole approximation[23] which is; $r = L \cos^2 \lambda$ gives,

$$dr = 2L \cos\lambda \sin\lambda \, d\lambda$$

substituting into equation (3) and rearranging gives the relationship

$$d\ell = L \cos\lambda \sqrt{4 - 3\cos^2\lambda} \quad d\lambda$$

substituting this relationship into equation (2) gives for a given L line

$$\bar{\rho} = \frac{\int \rho(B,L) \cos\lambda \sqrt{4 - 3\cos^2\lambda} \quad \frac{d\lambda}{\cos\alpha}}{\int \cos\lambda \sqrt{4 - 3\cos^2\lambda} \quad \frac{d\lambda}{\cos\alpha}} \tag{4}$$

From the conservation of magnetic moment[23] the relationship between B and α is

$$\frac{B}{B_e} = \frac{\sin^2\alpha}{\sin^2\alpha_e}$$

where subscript e refers to equator. Manipulation of above equation gives

$$\cos\alpha = \sqrt{1 - \frac{B}{B_e}\sin^2\alpha_e}$$

substituting this into equation (4) gives

$$\bar{\rho} = \frac{\int \frac{\rho(B) \cos\lambda \sqrt{4 - 3\cos^2\lambda} \quad d\lambda}{\sqrt{1 - B/B_e \sin^2\alpha_e}}}{\int \frac{\cos\lambda \sqrt{4 - 3\cos^2\lambda}}{\sqrt{1 - B/B_e \sin^2\alpha_e}} \quad d\lambda} \tag{5}$$

Notice, L has been dropped since the value of ρ will be done for a given L. Using the dipole approximation for B in terms of λ which is

$$B = \frac{M}{r^3}\left(1 + 3\sin^2\lambda\right)^{1/2}$$

where M is the earth's dipole moment (8.1×10^{25} gauss-cm^3)

Substituting

$$\frac{r}{r_e} = L\cos^2\lambda \quad \text{and} \quad \sin^2\lambda = 1 - \cos^2\lambda$$

gives

$$B = \frac{M\left(4 - 3\cos^2\lambda\right)^{1/2}}{r_e^3 L^3 \cos^6\lambda} \tag{6}$$

where r_e is the equatorial radius of the earth ($6.378.2 \times 10^5$ cm).

Assuming the starting point, a mirror point, there exist from the conservation of the magnetic moment the relationship

$$\sin^2\alpha_e = \frac{B_e}{B_o}$$

Substituting the equation for B in terms of λ gives

$$\frac{B}{B_o} = \sqrt{\frac{4 - 3\cos^2\lambda}{4 - 3\cos^2\lambda_o}}\left(\frac{\cos\lambda_o}{\cos\lambda}\right)^6$$

where subscript $_o$ refers to mirror point. Using the above relationships it turns out that

$$\sqrt{1 - \frac{B}{B_e}\sin^2\alpha_e} =$$

$$\left[\frac{\cos^6\lambda\,(4-3\cos^2\lambda_0)^{1/2} - \cos^2\lambda_0\,(4-3\cos^2\lambda)^{1/2}}{\cos^3\lambda\,(4-3\cos^2\lambda_0)^{1/4}} \right]^{1/2}$$

Substituting the above into equation (5) and replacing B in ρ by λ by equation (6) gives

$$\bar{\rho} = \frac{\displaystyle\int \frac{\rho(\lambda)\cos^4\lambda\sqrt{4-3\cos^2\lambda}\;d\lambda}{\sqrt{\cos^6\lambda\,(4-3\cos^2\lambda_0)^{1/2} - \cos^6\lambda_0\,(4-3\cos^2\lambda)^{1/2}}}}{\displaystyle\int \frac{\cos^4\lambda\sqrt{4-3\cos^2\lambda}\;d\lambda}{\sqrt{\cos^6\lambda\,(4-3\cos^2\lambda_0)^{1/2} - \cos^6\lambda_0\,(4-3\cos^2\lambda)^{1/2}}}}$$

letting

$$a = \sqrt{4-3\cos^2\lambda_0}$$

$$b = \cos^6\lambda_0$$

and defining the "weighing" factor

$$A(\lambda) = \cos^4\lambda \left[\frac{4-3\cos^2\lambda}{a\cos^6\lambda - b\sqrt{4-3\cos^2\lambda}} \right]^{1/2}$$

then, the "bounce" average, weighed over latitude, for a given field line is:

$$\bar{\rho} = \frac{\int_0^{\lambda_0} \rho(\lambda) A(\lambda)\, d\lambda}{\int_0^{\lambda_0} A(\lambda)\, d\lambda} \qquad (7)$$

The "weighing" factor, A (λ), appears in the averaging equations due to the fact that particles spiral about the field line in such a fashion as to stay longer at some latitudes, namely, near mirror latitudes, λ_0. Figure A-II is a plot of A (λ) versus λ for different mirror latitudes, λ_0. As can be seen from this figure, A (λ) is very large near λ_0 becoming indeterminant at λ_0. Notice the unusual dipping of the curves which occurs at $\lambda > 35^\circ$ for large mirror latitudes. This phenomena occurs principally because the line of force becomes relatively steep at large latitudes. For an equal $\Delta\lambda$, it turns out that the particle will spend less time at some large angles than at the equator. To elaborate, assume the mirror latitude is very high such that the pitch angle at the equator $\alpha_e \approx 0$. By comparing equations (5) and (1), one finds that

$$\frac{ds}{d\lambda} = A(\lambda) \approx \cos\lambda \sqrt{4 - 3\cos^2\lambda}$$

To find the point of inflection of A (λ) the derivative with respect to λ is set equal to zero:

$$\frac{d\,A(\lambda)}{d\lambda} = 0 = 3\cos^2\lambda - (4 - 3\cos^2\lambda)$$

solving for λ, find that

$$\lambda \approx 35^\circ$$

Checking with figure A-II, one sees that in this area the curve begins to dip. To find the time spent per path length consider

$$v_{\parallel} = \frac{ds}{dt} = \frac{ds}{d\lambda}\frac{d\lambda}{dt}$$

Or that,

$$\frac{dt}{d\lambda} = \frac{A(\lambda)}{v_{\parallel}}$$

Substituting the relationship of the total velocity into this equation gives

$$\frac{dt}{d\lambda} = \frac{A(\lambda)}{v\cos\alpha}$$

At the equator assuming the pitch angle $\alpha_e \gtrsim 0$, the time spent per path length is approximately

$$\left(\frac{dt}{d\lambda}\right)_e \approx \frac{1}{v}$$

Whereas at $\lambda > 35^\circ$ where the pitch angle is still very near zero, the time spent per path length is greater than 1/v since $A(\lambda > 35^\circ)$ is less than one.

The evaluations of the integrals are done numerically on an IBM 7090 digital computer using Simpson's technique[21]. At mirror latitudes, λ_0, the expression $A(\lambda_0)$ is undefined. In order to overcome this difficulty, equation (7) is numerically integrated from 0 to λ_0-E where E is made arbitrarily small such that the value of the integrals do not change appreciably.

APPENDIX B

A brief discussion on the motion of trapped particles in a magnetic field is presented in the appendix. Much of the material contained in this section comes from Singer and Lencheck[23], Jackson[23] and Spitzer[25]. This subject is reviewed so as to give completeness to the averaging process discussed in the analysis and calculation section.

Consider a charged particle of mass m and charge q in a magnetic field $\bar{B}$. The equations of motion for the particle can be written as

$$\frac{d\bar{p}}{dt} = \bar{F} = q(\bar{v} \times \bar{B}) \tag{1}$$

where $\bar{p}$ is the particle's momentum ($m\bar{v}$) and $\bar{F}$ is the Lorentz force exerted on the charge by the field. For simplicity purposes, relativistic mechanics will not be considered, since the effects to be pointed out are not relativistic. The scalar product of $\bar{v}$ with equation (1) shows that the kinetic energy of the particle is conserved. That is,

$$\frac{d}{dt}\left(\frac{1}{2}mv^2\right) = 0 \tag{2}$$

Equations (1) and (2) represent the equations of a trapped particle in a general magnetic field. To solve them one must specify the field B. Two spatial dependent fields are investigated to bring out particular points of the particle's motion utilized in the development of the average atmosphere. First will be a constant magnetic field, that is, B = constant. Secondly, a slowly spatial varying field.

Let the constant field $\bar{B}$ have magnitude B and be in the direction of the z axis. That is

$$\bar{B} = B\,\hat{\epsilon}_3$$

Consider velocity components $\parallel$ and $\perp$ to the $\bar{B}$ field such that the resultant velocity is of the form

$$\bar{V} = V_1\,\hat{\epsilon}_1 + V_2\,\hat{\epsilon}_2 + V_{\parallel}\,\hat{\epsilon}_3$$

By evaluating the cross-product of the right hand side of the equations of motion, the components of the equations of motion can be written as,

$$\frac{dV_1}{dt} = V_2\,\frac{B}{qm}$$

$$\frac{dV_2}{dt} = -V_1\,\frac{B}{qm}$$

$$\frac{dV_{\parallel}}{dt} = 0$$

It is seen that the component of velocity parallel to the magnetic field is a constant of the motion. By differentiating with respect to time the first component of the acceleration equation and substituting into the second gives

$$\frac{d^2 v_1}{dt^2} + \left(\frac{B}{qm}\right)^2 v_1 = 0$$

A solution to the differential equation is

$$v_1 = C e^{-i w_B t}$$

where C is a constant of integration to be evaluated and where w_B is defined as B/qm. Differentiating the solution of v_1 and substituting it back into the first equation gives the velocity component,

$$v_2 = -iCe^{-i w_B t}$$

Considering the real part of the solutions shows the velocity component $\perp$ to $\bar{B}$ to be

$$v_1 = C \cos w_B t$$

$$v_2 = -C \sin w_B t$$

To evaluate the constant C, one realizes that the centripetal acceleration equals the Lorentz force. That is,

$$\frac{v_\perp^2}{a} = \frac{v_\perp q B}{m} = v_\perp w_B \qquad (3)$$

where a is the radius of the circle. The value of the velocity $\perp$ to the field is

$$v_\perp = w_B a$$

From the solution of the equations of motion,

$$V_\perp = \sqrt{V_1^2 + V_2^2} = C$$

Thus, the constant of integration is

$$C = w_B a$$

The complete solution of the equations of motion for the velocity is

$$\bar{V} = w_B a \left(\cos w_B t \, \hat{\epsilon}_1 - \sin w_B t \, \hat{\epsilon}_2 \right) + V_{\parallel} \hat{\epsilon}_3$$

where;

$v_{\parallel}$ is a constant velocity in the direction of $\bar{B}$, that is, along the z-axis

a is the radius of gyration about the z-axis

w_B is called the gyration frequency

The circular motion with velocity v in the xy plane combined with the translation along the z-axis results in a helix. The gyro-period about the z-axis is

$$t_g = \frac{2\pi a}{V_\perp}$$

Using equations (3), this can be written as

$$t_g = \frac{2\pi}{w_B}$$

From equation (3) it is seen that the pitch angle, α (defined as the angle between $\bar{v}$ and $\bar{B}$) is constant throughout the trajectory for a constant B field. The magnitude of α is

$$\alpha = \sin^{-1}\left(\frac{qBa}{mv}\right)$$

Another important parameter used in magnetostatic motion is the magnetic moment, μ. It is defined as the current times the area enclosed, that is,

$$\mu = I\,(\text{Area})$$

For a particle of charge q traveling in a circle or radius a with velocity $v_\perp$,

$$I = q \times (\text{number of gyrations/sec}) = q\,\frac{w_B}{2\pi}$$

Substituting into the definition and using equation (3), it turns out that

$$\mu = \frac{\frac{1}{2} m v_\perp^2}{B} \qquad (4)$$

For a constant field, μ is also a constant of the motion.

A spatial variation in the magnetic field causes the particle to drift. The drift of a particle due to the inhomogeniety of the field is usually broken down into two cases. First, the drift due to the field change (∇B) as the particle spirals about a field line, and secondly, the drift due to the curvature of the field. The development of the gradient drift is usually done by an approximation.

That is, by expanding $\bar{B}$ in a Taylor series about the center of gyration and keeping only the first two terms. The criteria of the expansion is that

$$\left| \frac{\nabla B}{B} \right| \ll \frac{1}{a} \tag{5}$$

or that the field doesn't change very much compared to the radius of gyration, a. The motion is again broken into two components, $\parallel$ and to $\bar{B}$. Since the direction of $\bar{B}$ is unchanged, the motion $\parallel$ to $\bar{B}$, still a uniform translation, will be unchanged. The necessary modification to the trajectory comes from $v_\perp$. That is, a transverse precession velocity is calculated[24] as

$$\bar{V}_G = \frac{w_B a^2}{2B^2} \left(\bar{B} \times \nabla_\perp B \right) \tag{6}$$

as can be seen, the drift velocity if perpendicular to both. $\bar{B}$ and $\nabla_\perp B$.

Before considering the curvature drift velocity, there is an important point to be made at this time. From Spitzer[25], it turns out that μ is a constant of the motion if B doesn't change appreciably for a change in distance equal to a. That is

$$\mu = \frac{\frac{1}{2} m v_\perp^2}{B} = \text{constant}$$

This leads to the mirroring motion of particles. That is, μ can be written in terms of total energy and pitch angle as

$$\mu = \frac{\frac{1}{2} m v^2 \sin^2\alpha}{B} = \text{constant}$$

This is true for all points. A relation can be established for an arbitrary point. That is,

$$\frac{\sin^2\alpha}{B} = \frac{\sin^2\alpha_o}{B_o}$$

or,

$$\sin\alpha = \frac{B}{B_o}\sin\alpha_o$$

when $\frac{B}{B_o}$ reaches $\frac{1}{\sin \alpha_o}$, $\sin \alpha = 1$. Or, in terms of velocity, all of the velocity is $V_\perp$, and $V_\parallel$ falls to zero. At this point, the particle "reflects" and moves in the opposite direction. This motion is the basis of the fourth averaging process where the reflection point commonly referred to as the mirror point is used as a parameter of the study.

The drift due to the field curvature is treated in Jackson[24] and Singer and Lenchek[23]. The simplest approach[23] is to consider Lorentz'sforce equation,

$$\bar{F}/q = \bar{f} = \bar{v} \times \bar{B}$$

By assuming the force is much smaller than $\bar{B}$, then, to first order, the resulting velocity due to the perturbative force is

$$\bar{v}_f = \frac{\bar{f} \times \bar{B}}{B^2}$$

or, a force/unit charge $\bar{f}$ on a charged particle will produce a velocity $\bar{V}_f$ which is at right angles to $\bar{f}$ and $\bar{B}$. If the force is due to the curvature of the path, that is, the centripetal force $\frac{mV_{\parallel}^2}{R_c}$, the curvature drift velocity becomes from equation (7)

$$\bar{V}_c = \frac{mV_{\parallel}^2 \bar{R}_c \times \bar{B}}{qB^2 R_c^2} \tag{8}$$

If $\nabla \times \bar{B} = 0$, then $\frac{\bar{R}_c}{R_c^2} = -\left(\frac{\nabla_\perp B}{B}\right)$, or equation (8) becomes

$$\bar{V}_c = \frac{mV_{\parallel}^2 \bar{B} \times \nabla_\perp B}{qB^3} \tag{9}$$

Combining (6) and (9) and using equation (3), the total drift velocity becomes

$$\bar{V}_t = \frac{\bar{B} \times \nabla_\perp B}{qB^3} \left(\frac{1}{2} mV_\perp^2 + mV_{\parallel}^2 \right) \tag{10}$$

Equation (10) represents the total drift velocity due to the gradient and the curvature of the magnetic field. The drift is east to west for protons, or positive charged particles. The drift motion is the reason for the longitudinal averaging process in the construction of the atmosphere.

REFERENCES

1. Hess, W. N., "Van Allen Belt Protons Cosmic Ray Neutron Leakage" Phys. Review Letters, vol. 3, no. 1, July 1, 1959.

2. Pizzella, Guido, "Time Variations of Intensity in the Earth's Inner Radiation Zone" (October 1959 through December 1960) S. U. I.-62-1, Contract NAG W-17.

3. Harris, I, and Priester, W., "Theoretical Models for the Solar-Cycle Variation of the Upper Atmosphere" NASA, GSFC publ. X-640-62-70, June, 1962.

4. Harris, I., and Priester, W., "Time-Dependent Structure of the Upper Atmosphere", April, 1962, NASA, GSFC, Institute for Space Studies publication.

5. Aron, W. A., Hoffman, B. C., Williams, F. C., "Range-Energy Curves" (2nd Rev. 1949) U. S. A.E.C., Univ. of Calif. Rad. Lab.

6. Ray, Ernest C., "On the Theory of Protons Trapped in the Earth's Magnetic Field" J. of Geophys. Res., vol. 65, no. 4, April, 1960, pp. 1125-1133.

7. Freden, S., White, R., "Particle Fluxes in the Inner Radiation Belt" J. of Geophys. Res., vol. 65, no. 5, May, 1960.

8. Fermi, E., Orear, J., Rosenfeld, A. H., Schluter, R. A. "Nuclear Physics" (Revised Edition), Univ. of Chicago Press, copyright 1950.

9. Hess, W. N., "Energetic Particles in the Inner Van Allen Belt," Space Science Reviews, vol. 1, no. 2, October, 1962.

10. McIlwain, C. E., "Coordinates for Mapping the Distribution of Magnetically Trapped Particles, J. of Geophys. Res. vol. 66 (1961) pp. 3681-3691.

11. Jensen, D. C., and Cain, J. C., unpublished, presented at April, 1962, meeting of the American Geophysical Union, Washington, D. C.

12. Stassinopoulos, E. G., private communication.

13. Hess, W., Blanchard, R., and Stassinopoulos, E., private communicatior

14. McIlwain, C. E., Pizzella, G., "On the energy Spectrum of Protons Trapped in the Earth's Inner Van Allen Zone," to be published, under contract NASA-116.

15. Apel, J. R., Singer, S. F. and Wentworth, R. C., "Effects of Trapped Particles on the Geomagnetic Field," December, 1961, Contract AF-19 (604) 3861.

16. Singer, S. F., "Nature and Origin of Radiation Belts," Journal of The Physical Society of Japan, vol. 17 Supplement A-II 1962, p. 187.

17. Lencheck, A. M., and Singer, S. F., "Geomagnetically Trapped Protons from Cosmic Ray Albedo Neutrons," Journal of Geophys. Res. vol. 67, no. 4, April, 1962, p. 1263.

18. Freden, S. C., and White, R. S., "Trapped Proton and Cosmic-Ray Albedo Neutron Fluxes," J. of Geophys. Res., vol. 67, no. 1, January, 1962, p. 25.

19. McDonald, F., private communication.

20. McDonald, and Webber, "A study of the Rigidity and Charge Dependence of Primary Cosmic Ray Temporal Variations," Journal of the Physical Society of Japan, vol. 17, Supplement A-II, Proceedings of the International Conference on Cosmic Rays and the Earth Storm, September 4-15, 1961.

21. Scarborough, J. B., "Numerical Mathematical Analysis" 3th Edition, Oxford University Press, Copyright, 1955.

22. Evans, R. D., "The Atomic Nucleus" McGraw Hill Co., Copyright 1955.

23. Singer, S. F. and Lenchek, A. M., "Geomagnetically Trapped Radiation Physics Department, U. of Maryland, August, 1961, Tech. Report No. 2

24. Jackson, J. D., "Classical Electrodynamics," J. Wiley and Sons, Copyright 1962.

25. Spitzer, L., "Physics of Fully Ionized Gases" 2nd edition, Interscience, 1962.

26. Hess, W. N., "Radiation Belts," Transactions of the American Geophysical Union, Vol. 44, No. 2, June, 1963.

27. O'Brien, B. J., "Review of Studies of Trapped Radiation with Satellite-Borne Apparatus," Space Science Reviews, D. Reidel Publ. Co. Dordrecht-Holland.

28. Van Allen, J. A., "Current Work on Geomagnetically Trapped Corpuscular Radiation," I.C.S.U. Review, Vol. 3, No. 1, pp 53-60, Elsevier Publ. Co., Amsterdam.

29. Hess, Canfield, Lingenfelter, 1961, Cosmic Ray Neutron Demography, J. of Geophys. Res., vol. 66, p. 665.

ACKNOWLEDGMENTS

The author wishes to express his appreciation to Dr. W. N. Hess under whose direction, continued guidance, and advice this study was performed. The author also wishes to express his appreciation to Dr. D. Stern for his explanations of parts of the theory and helpful criticisms.

The author wishes to express special thanks to Mr. E. G. Stassinopoulos for his explanations of the B, L transformation program, to Marian Underwood and Dorothy Pollack for their typing efforts, and to Janice Chiville and Carol Lee Foley for preparing the final manuscript.

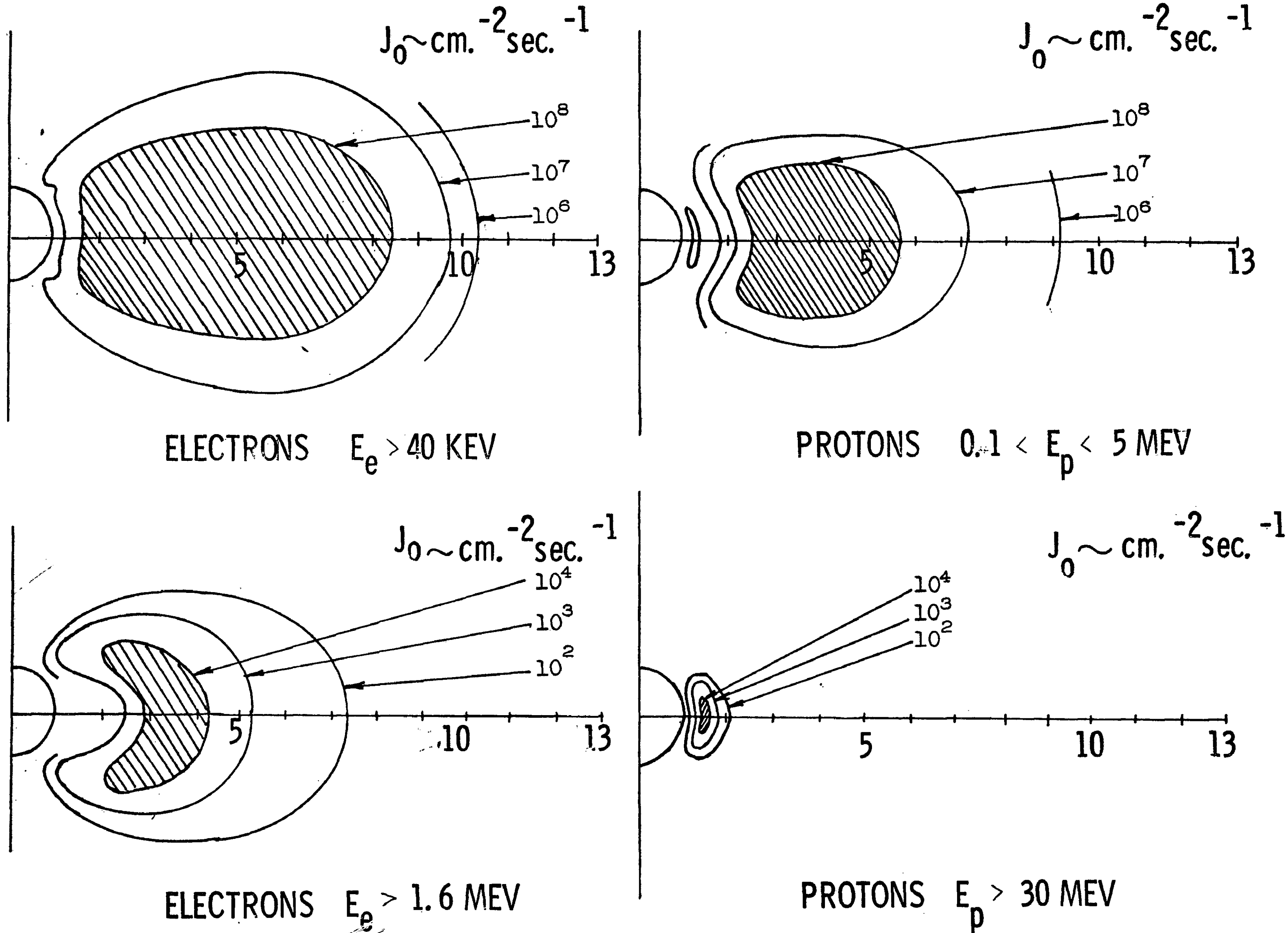

Figure I-1. Radiation belt description

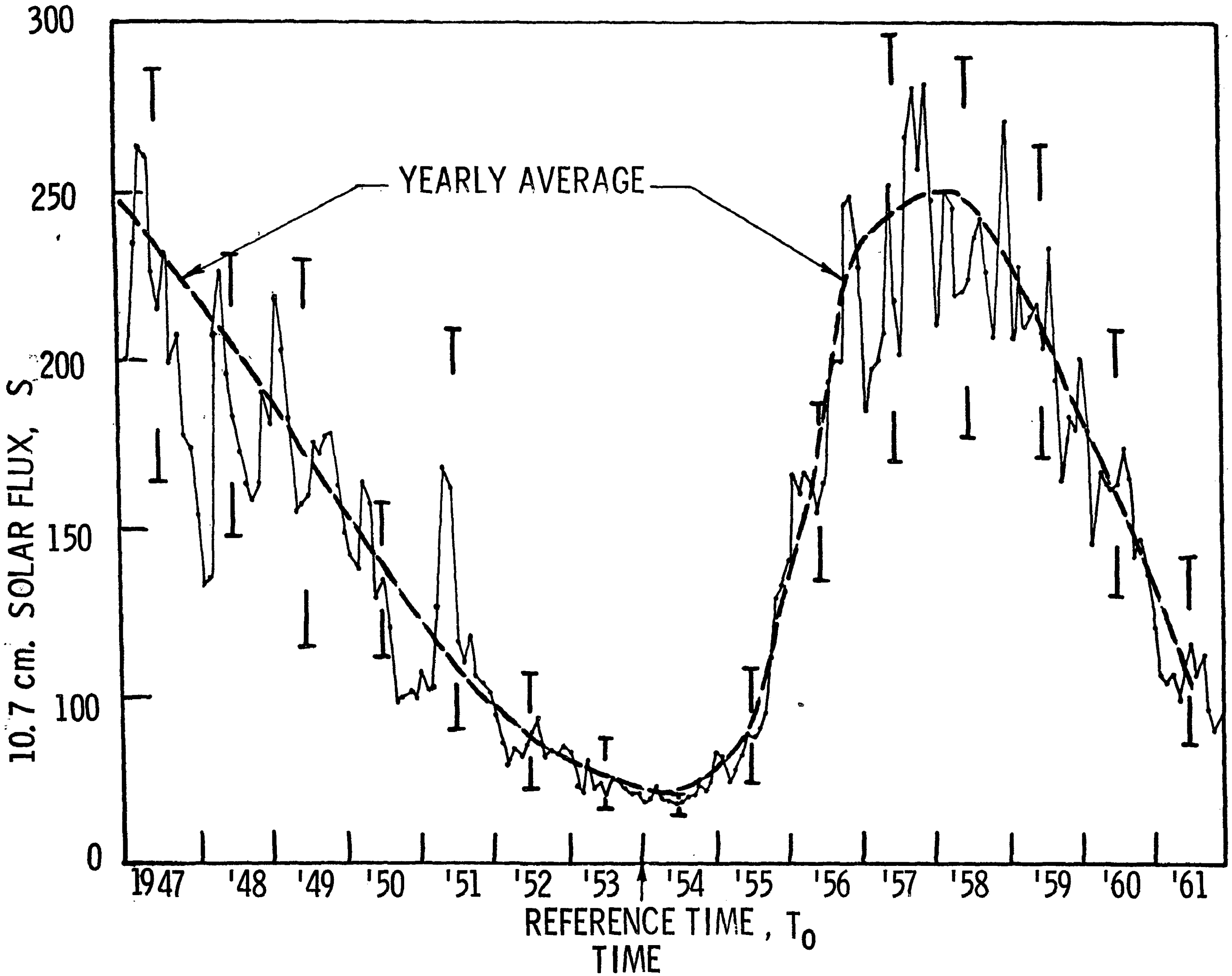

Figure 1. A time history of the 10.7 cm. solar flux according to the measurements of the National Research Council of Canada for the recent past. The heavy dotted line indicates the approximate yearly average.

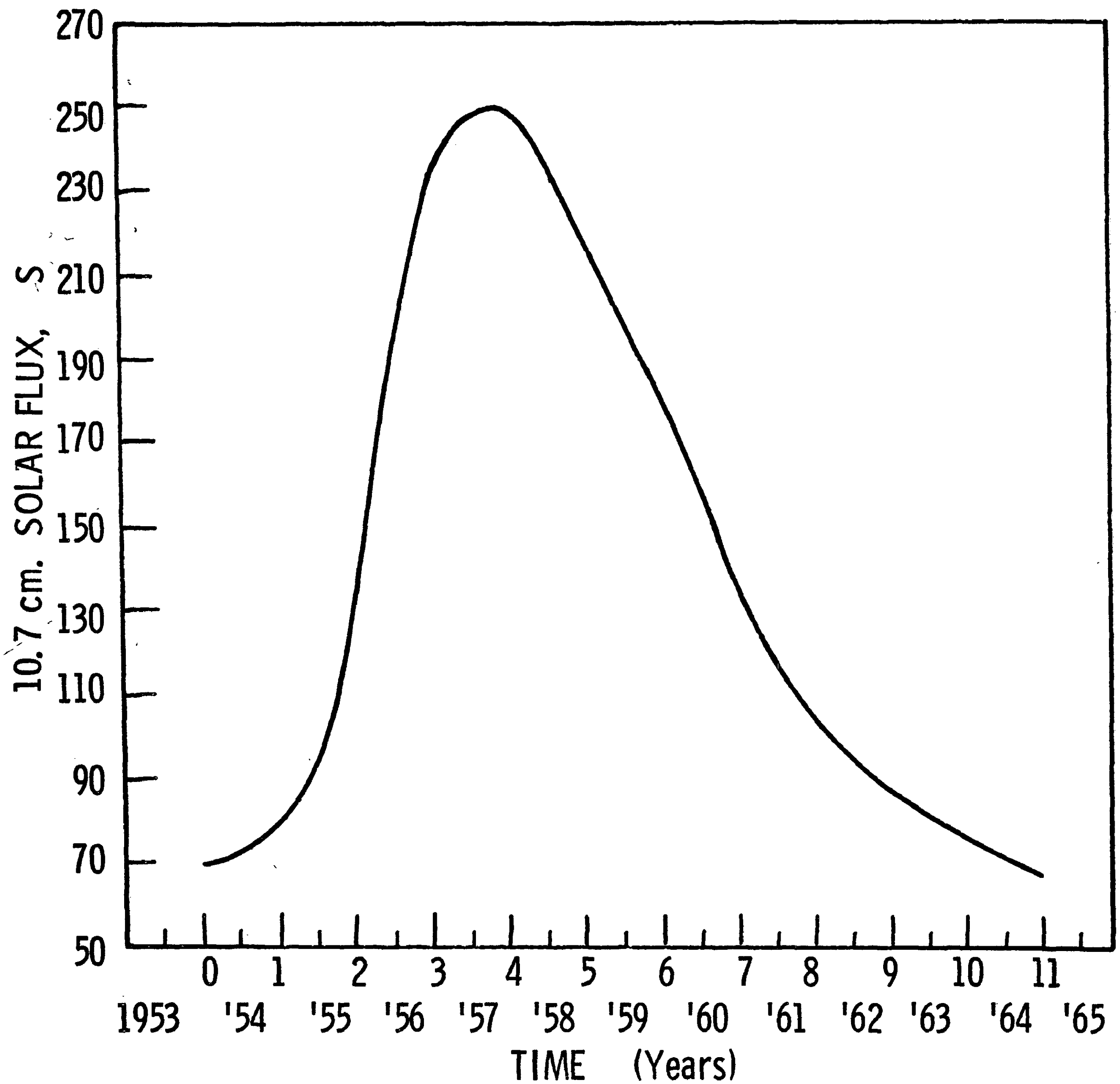

Figure 2. A time history of the constructed mean solar cycle variation of the 10.7 cm. solar flux with reference time t_o of Jan., 1954.

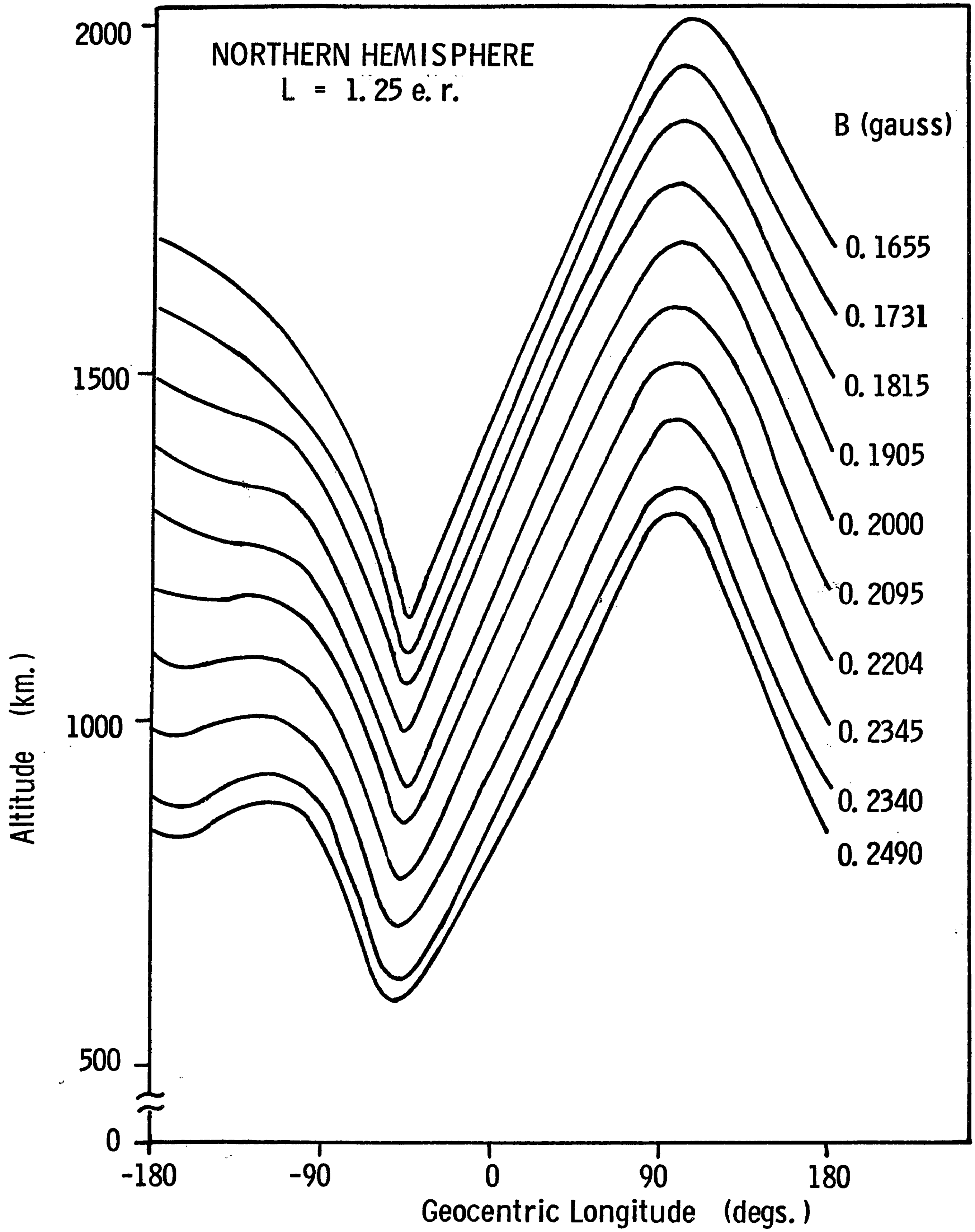

Figure 3. B contours at L=1.25 e.r. for the Northern Hemisphere of altitude and geocentric longitude.

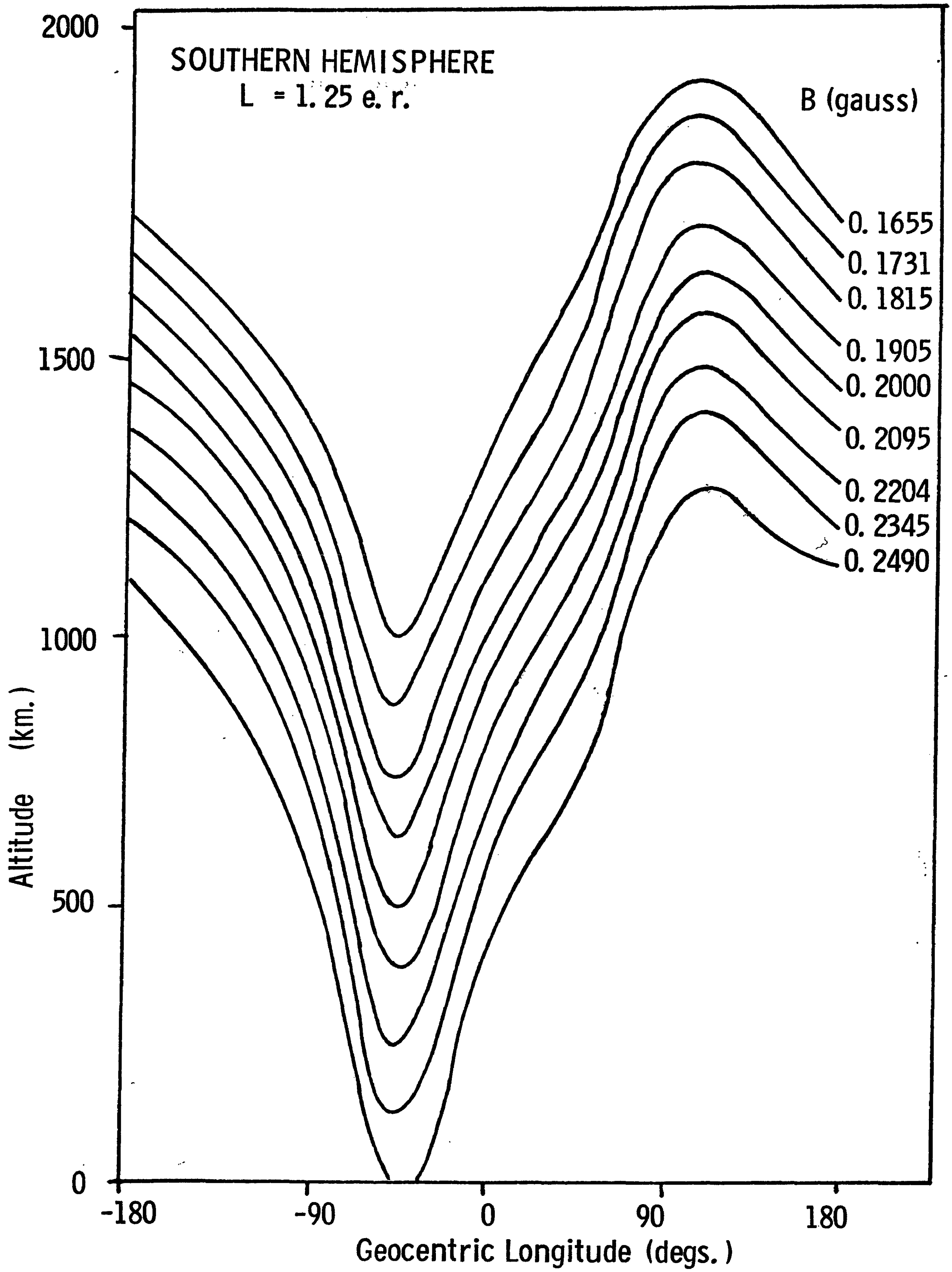

Figure 4. B contours for L=1.25 for the Southern Hemisphere as a function of altitude and geocentric longitude.

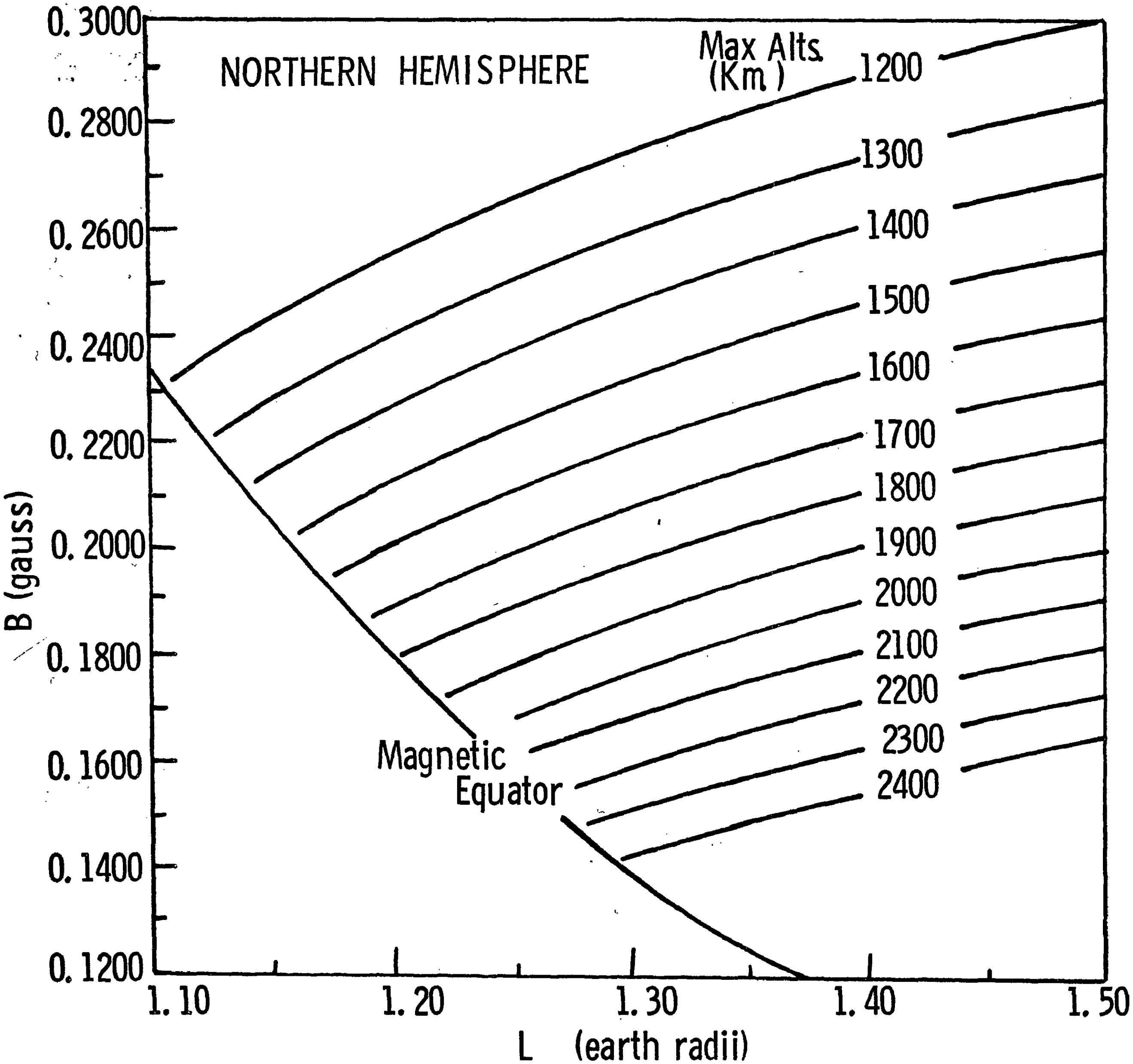

Figure 5. Maximum altitude contours in B, L space for the Northern Hemishpere.

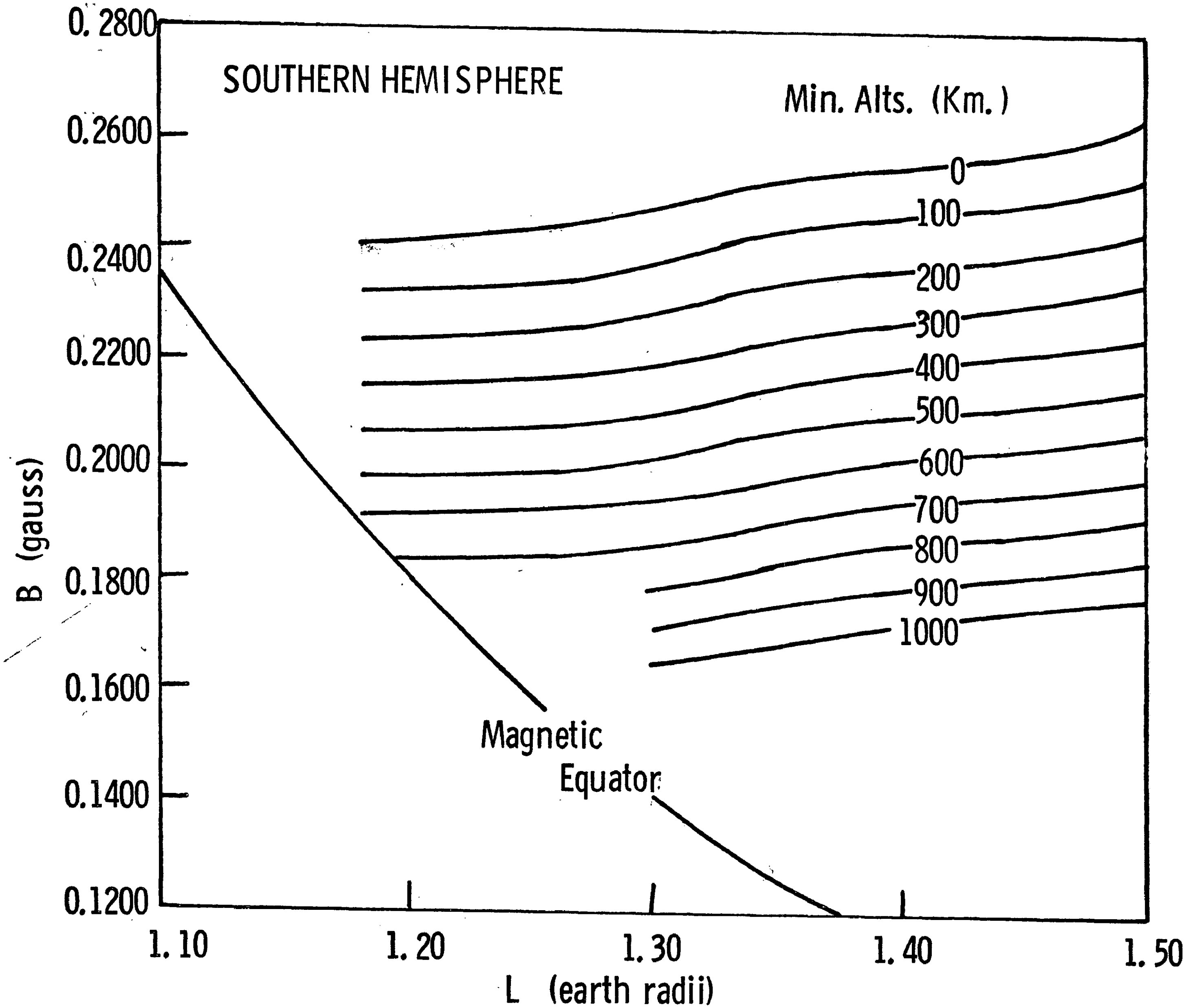

Figure 6. Minimum altitude contours in B, L space for the Southern Hemisphere.

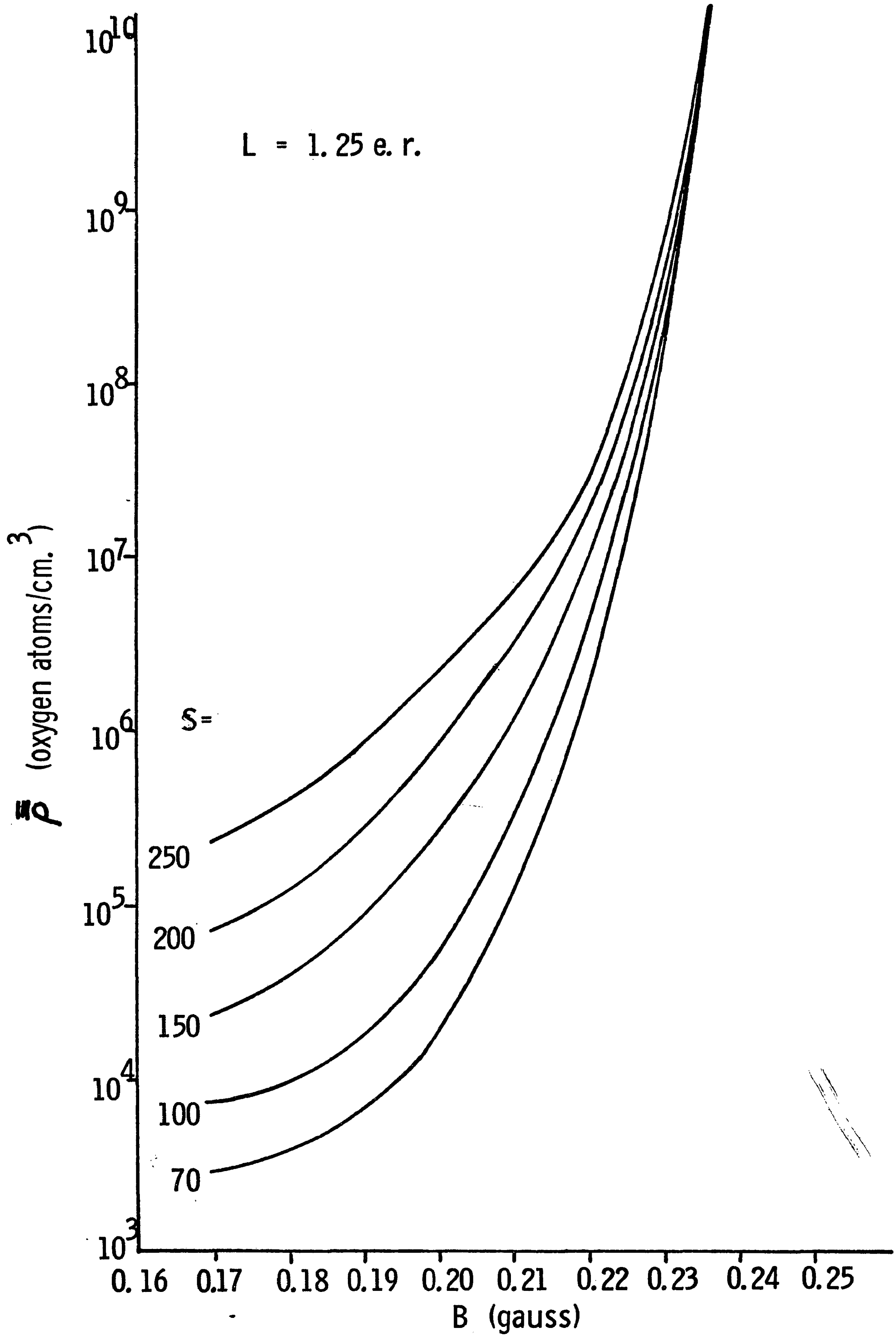

Figure 7. The average oxygen number density as a function of B for the five solar flux numbers at L=1.25

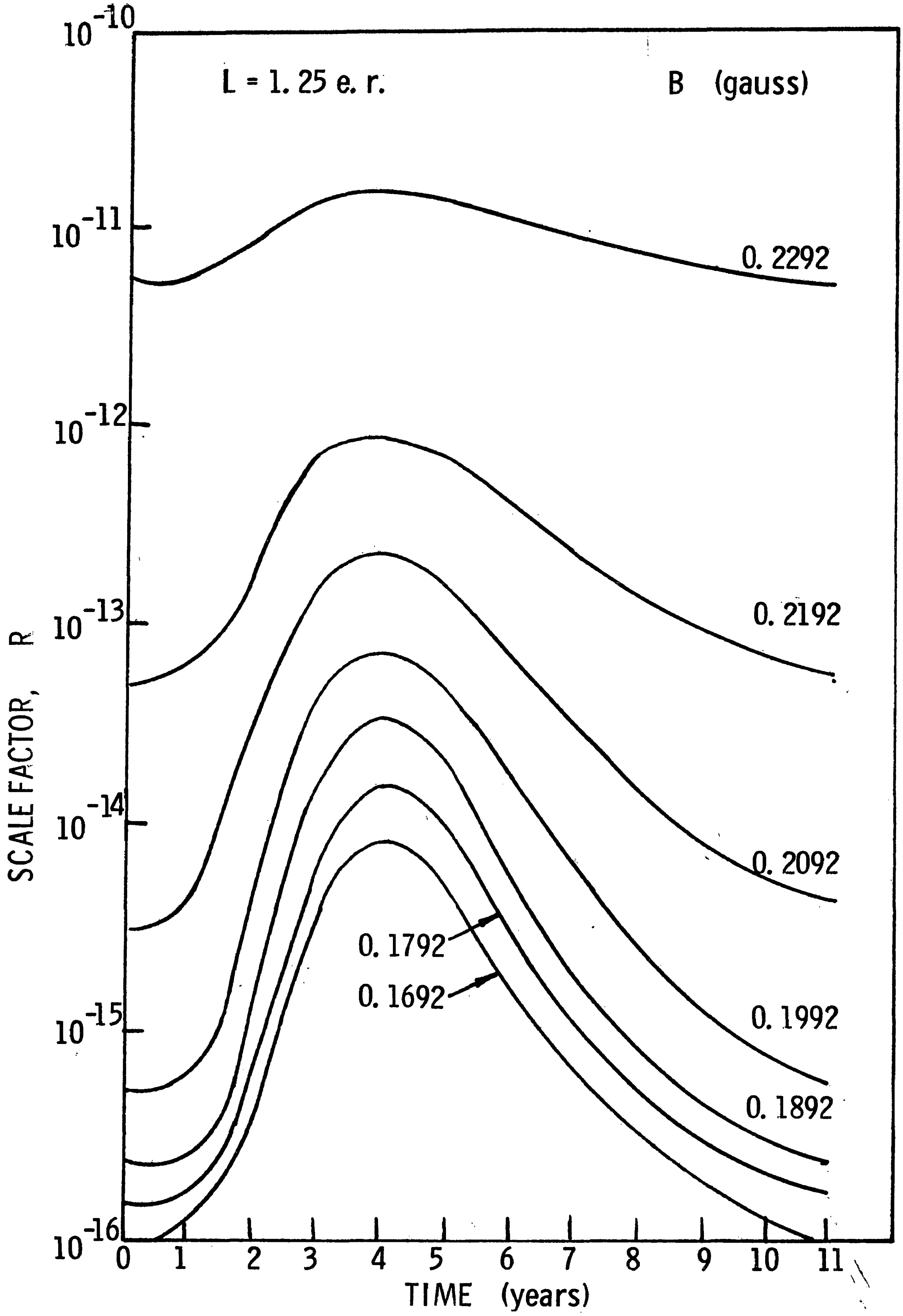

Figure 8. A time history of the atmosphere scale factor, R as a function of B at L = 1.25 e.r.

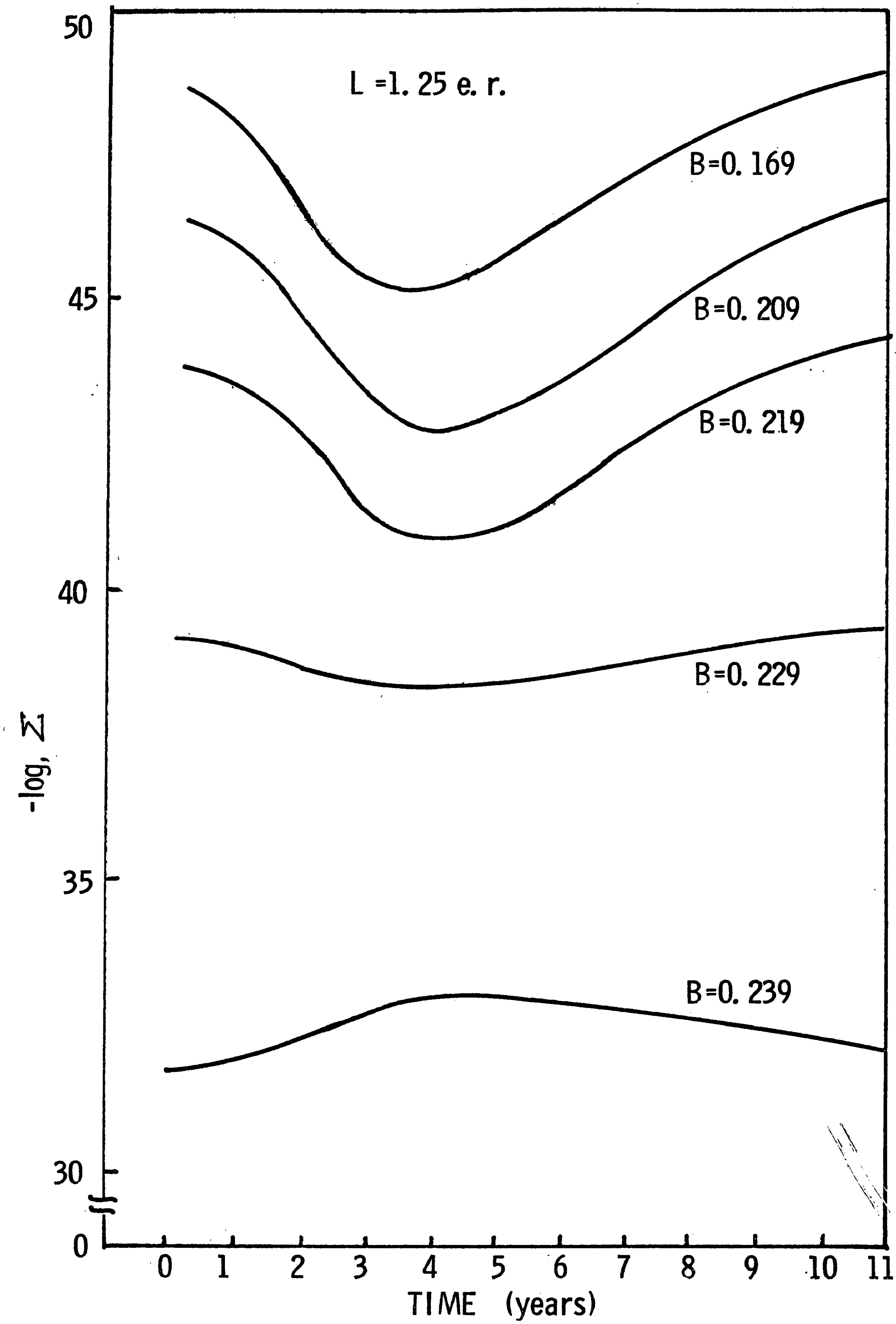

Figure 9. A time history of the "effective" cross-section of the atmosphere, Σ as a function of B at L=1.25 e.r.

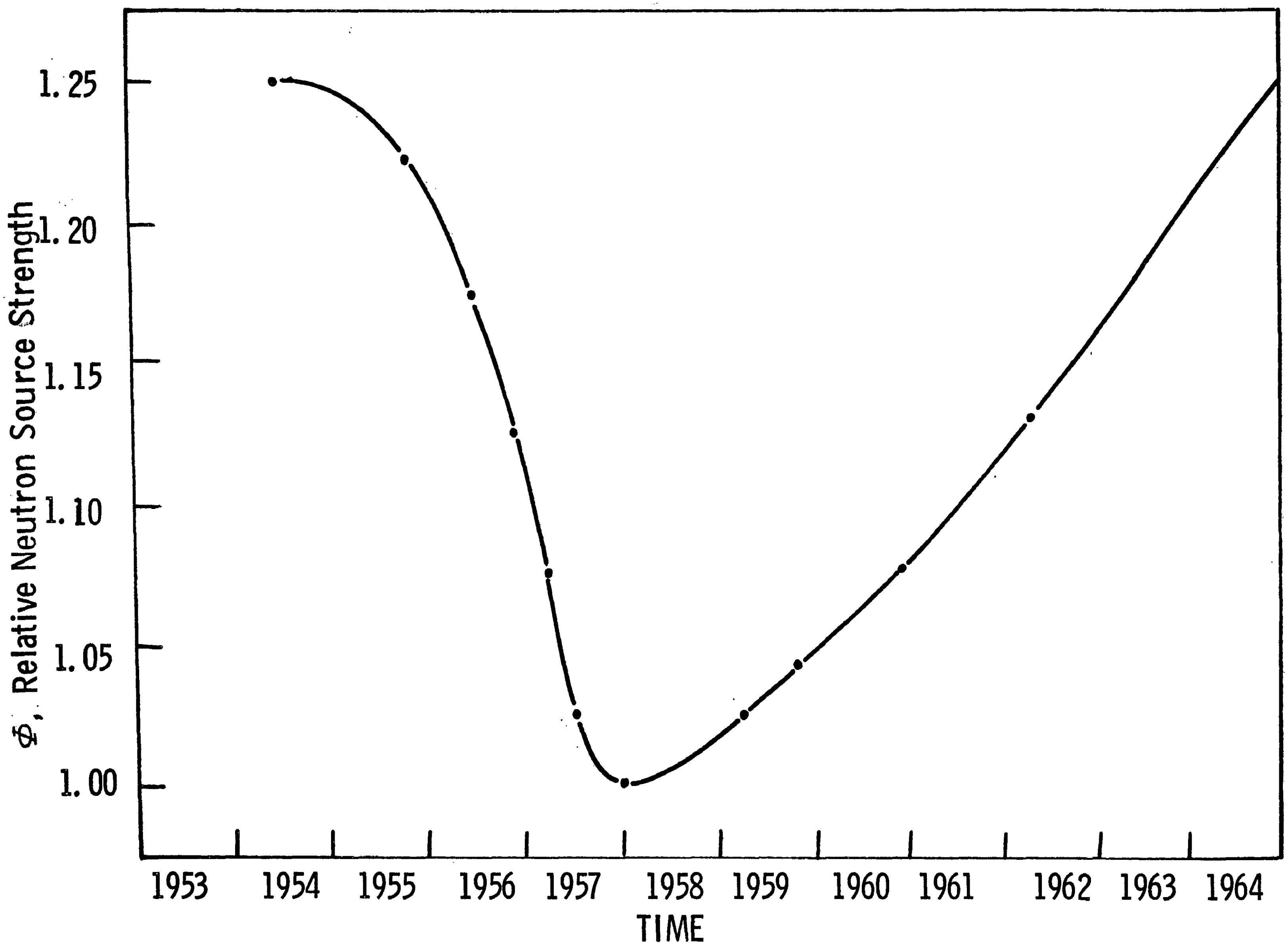

Figure 10. A time history of the relative inner belt source strength.

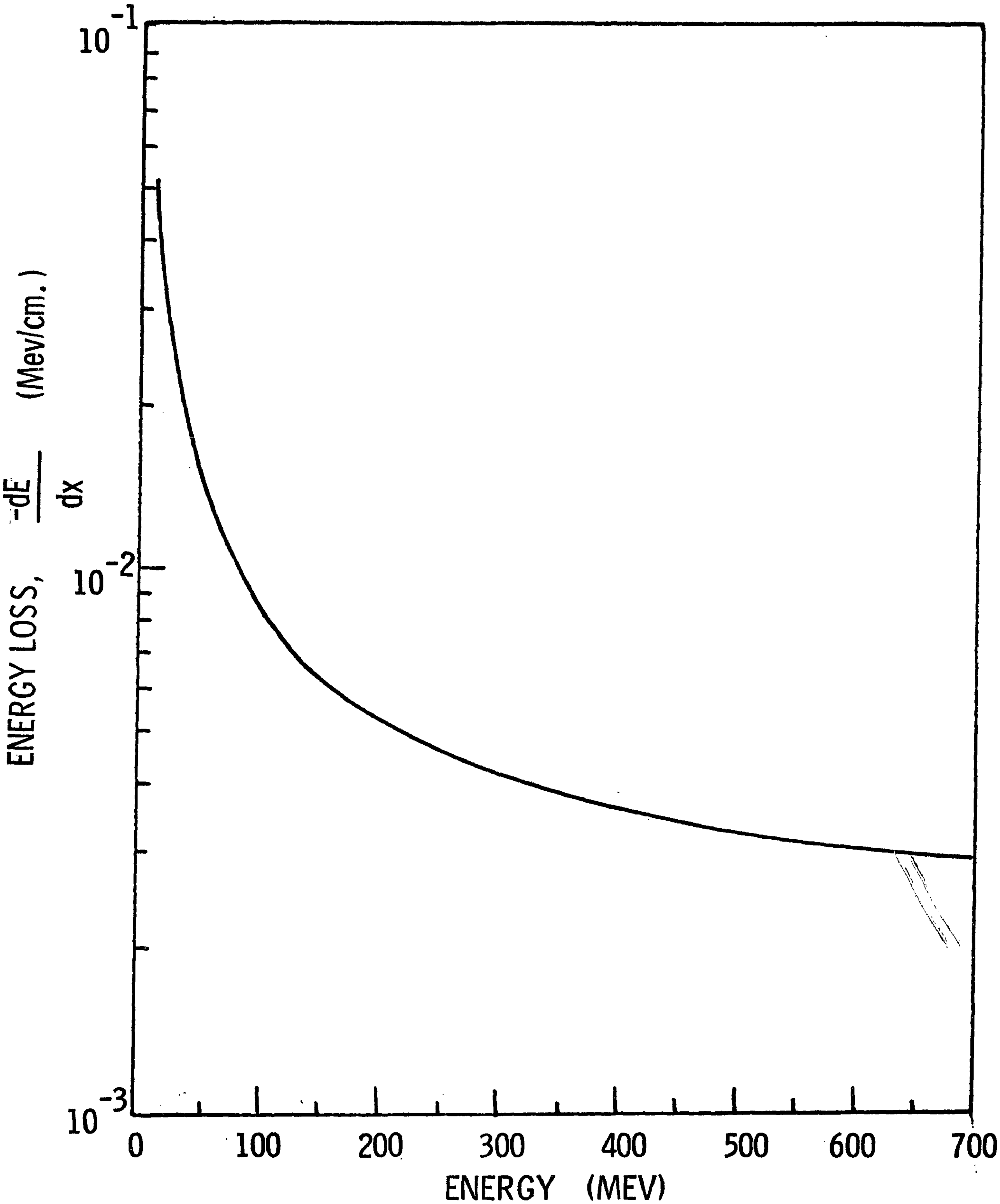

Figure 11. The proton energy loss spectrum for an oxygen target.

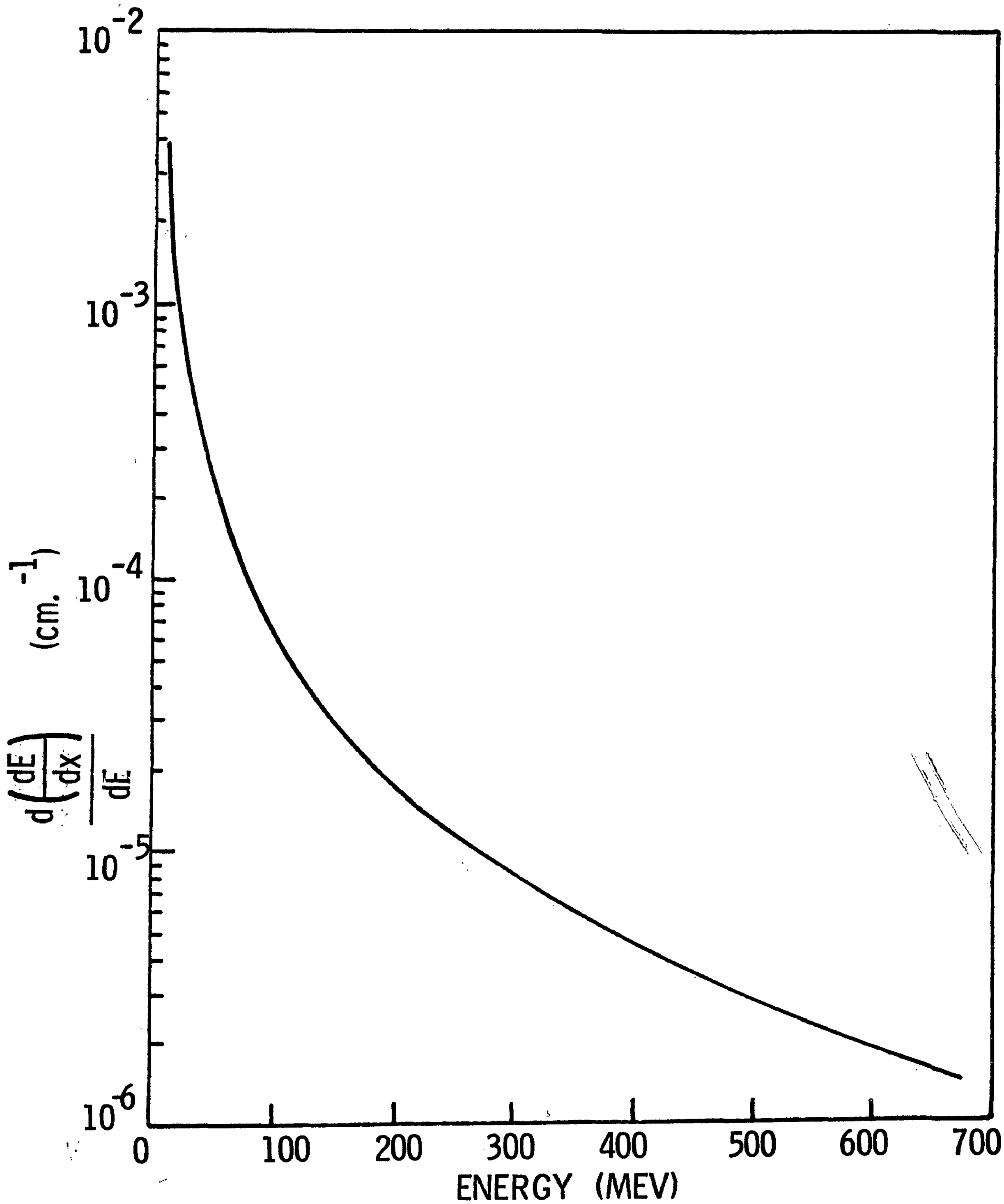

Figure 12. The slope of proton energy loss versus energy for an oxygen target.

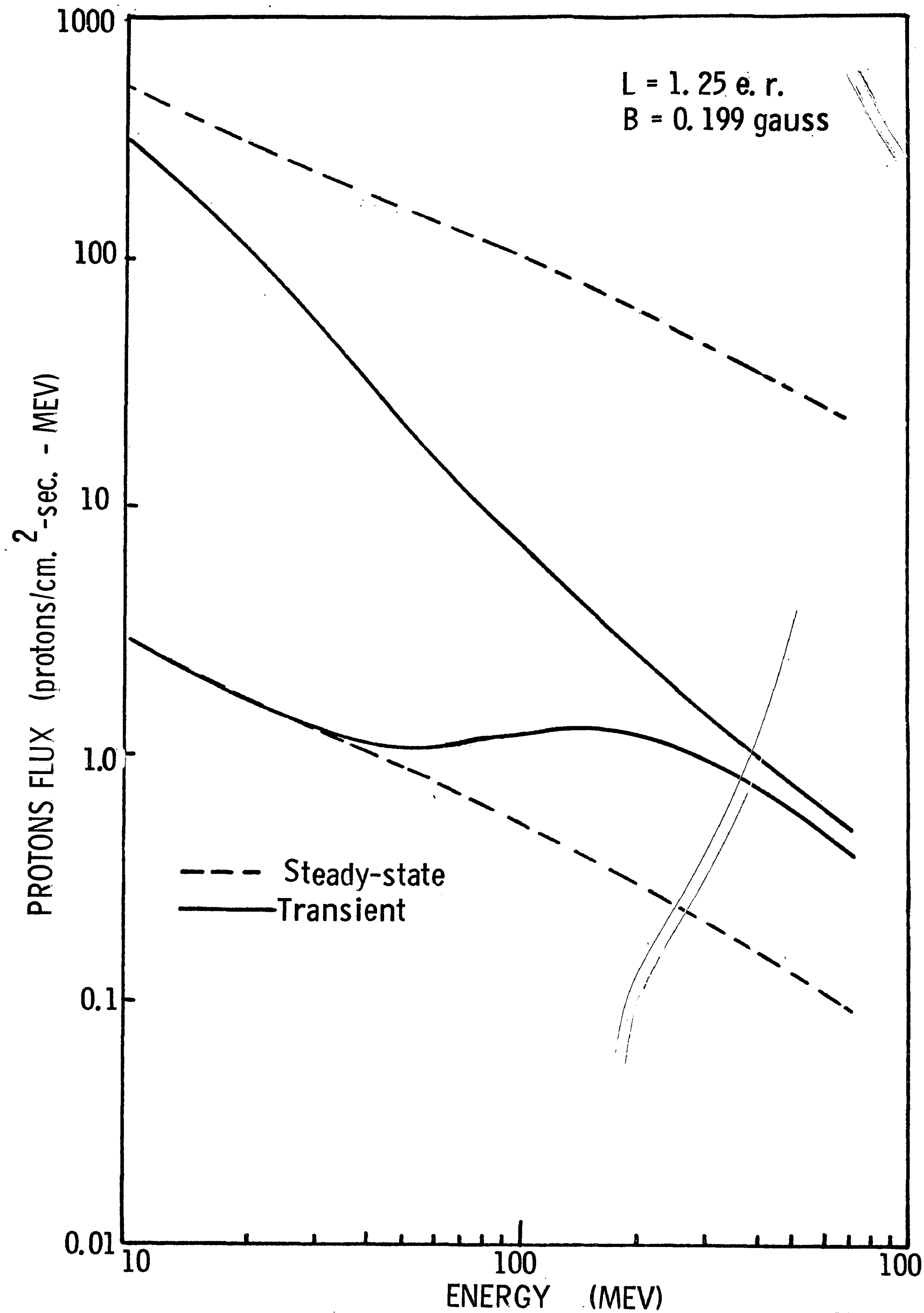

Figure 13. A comparison of the steady-state and transient proton flux energy spectrums for L = 1.25, B = .199 at solar minimum and solar maximum.

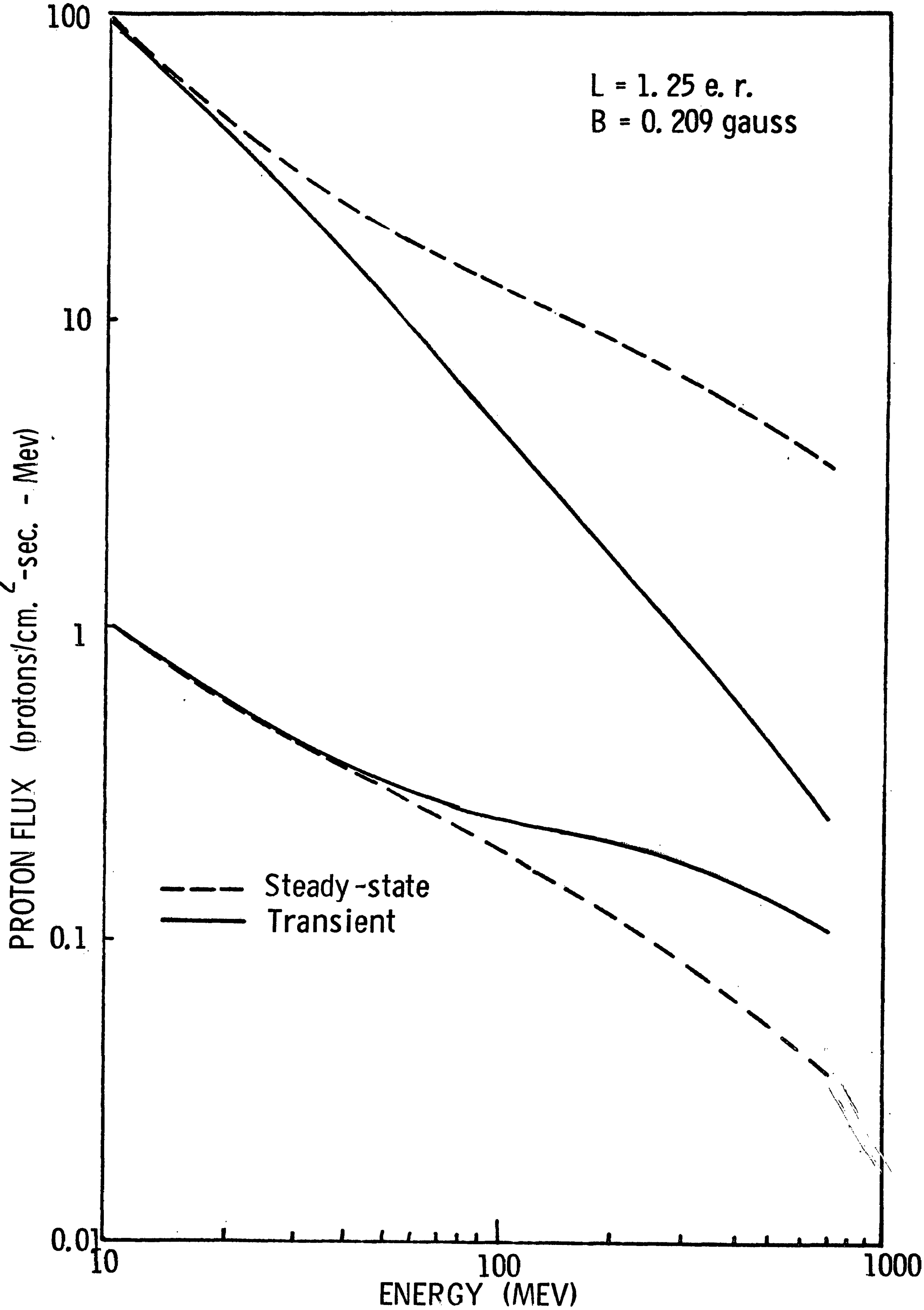

Figure 14. A comparison of the steady-state and transient proton flux energy spectrums for L=1.25, B=2.09 at solar minimum and solar maximum.

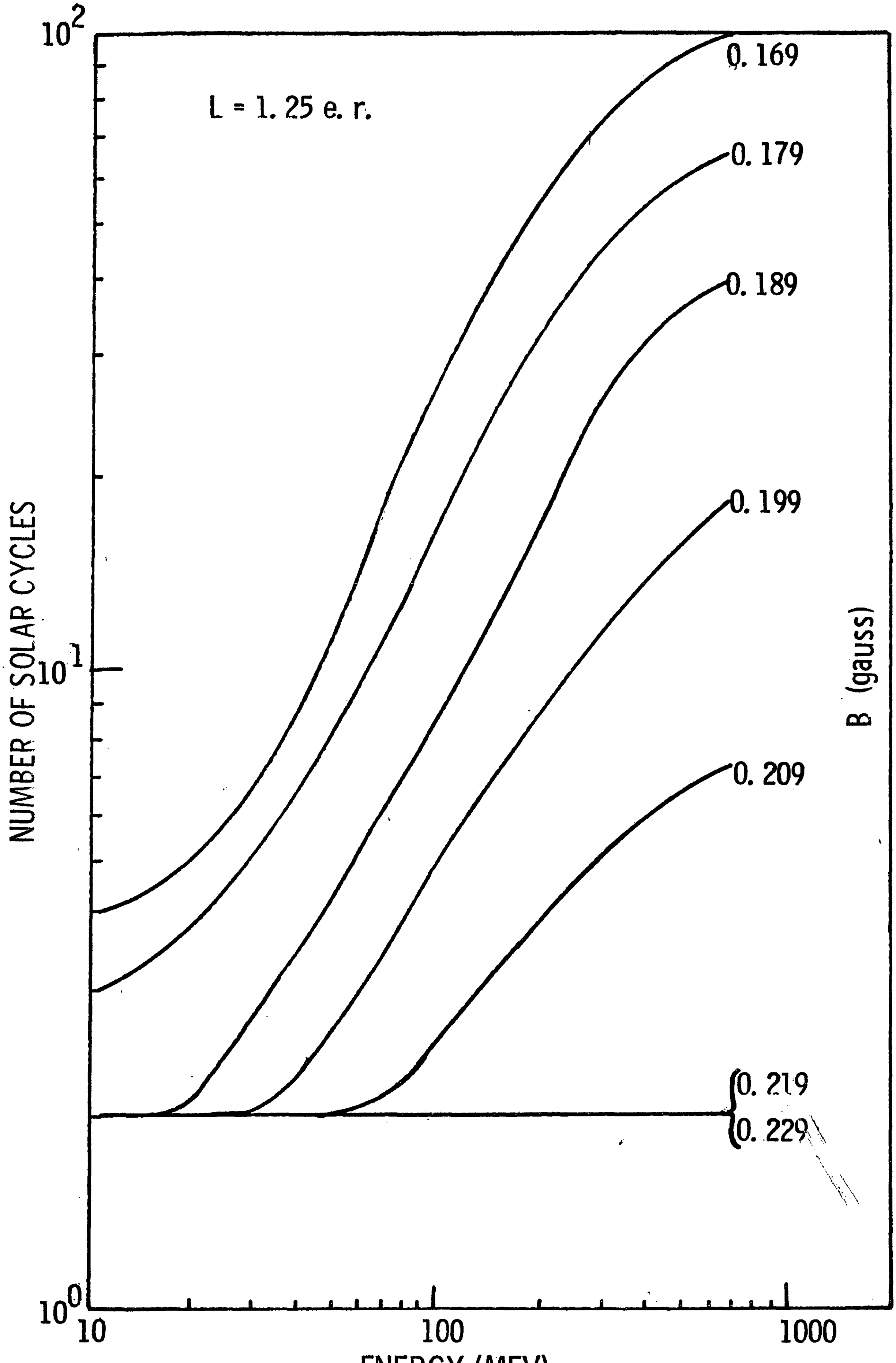

Figure 15. The time required in terms of solar cycles to build steady-state conditions versus energy as a function of B.

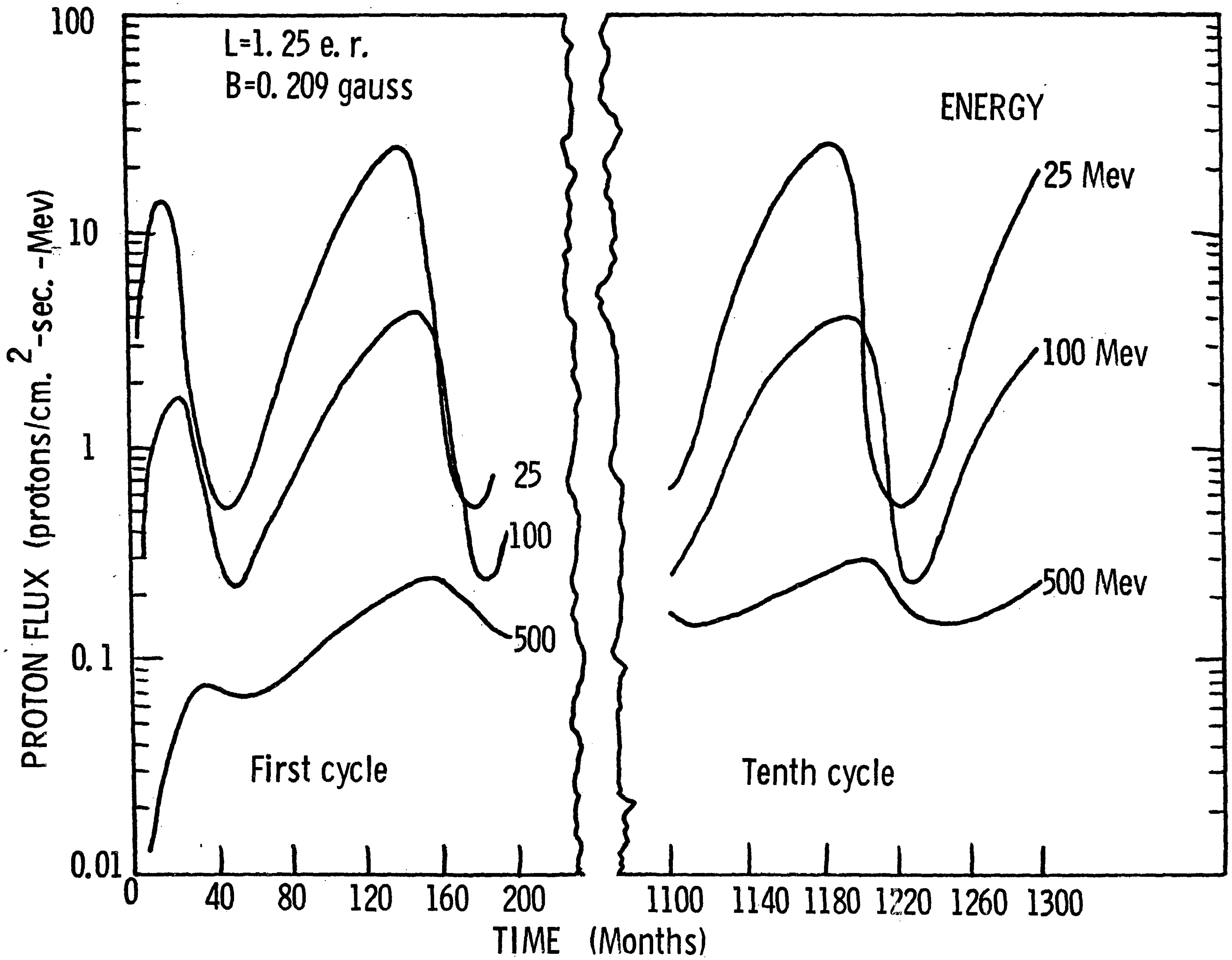

Figure 16. A time history of proton flux as a function of energy at L=1.25, B=.209 for the first and tenth solar cycles.

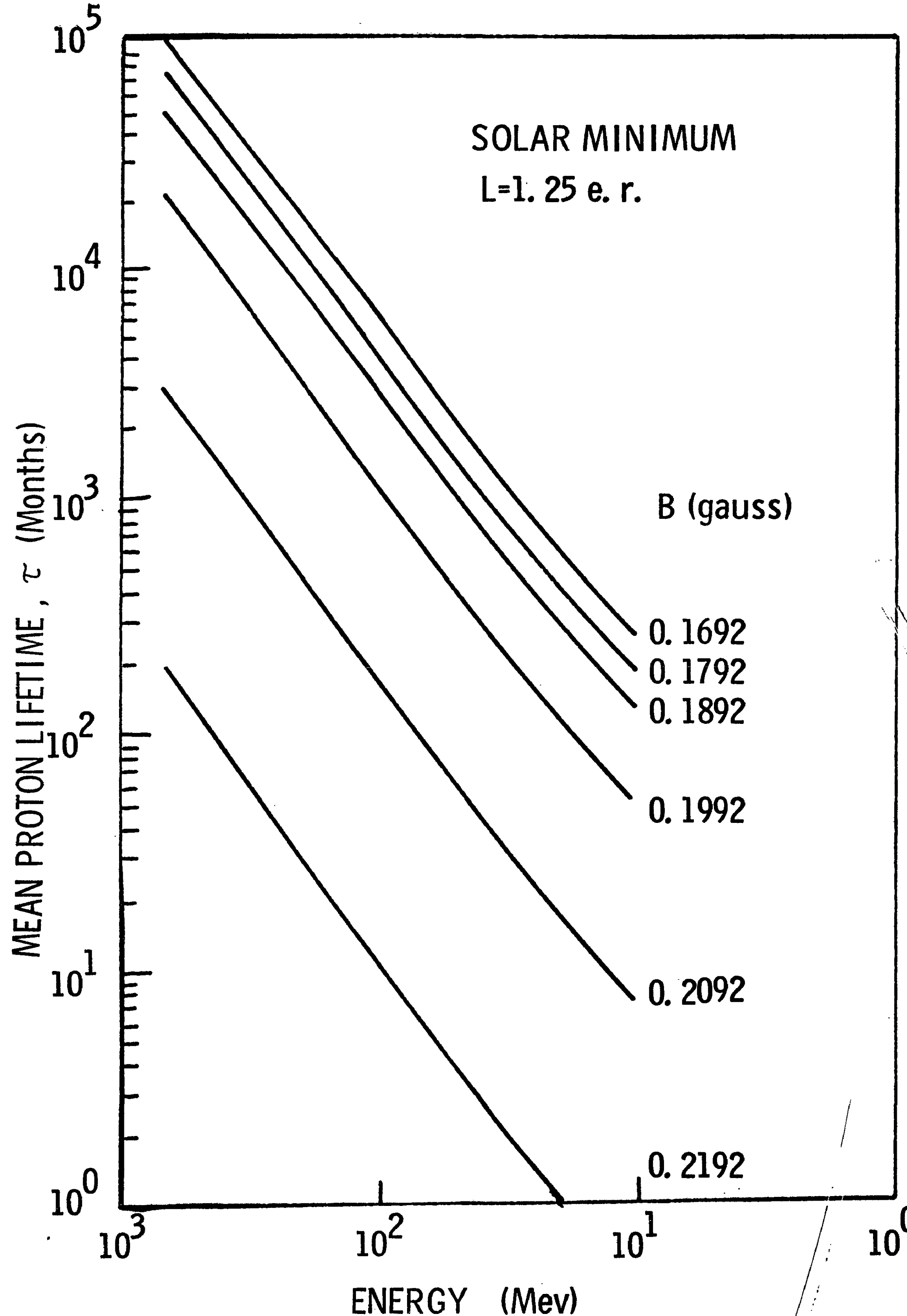

Figure 17. The mean proton lifetime, τ energy spectrum as a function of postion at solar mimimum.

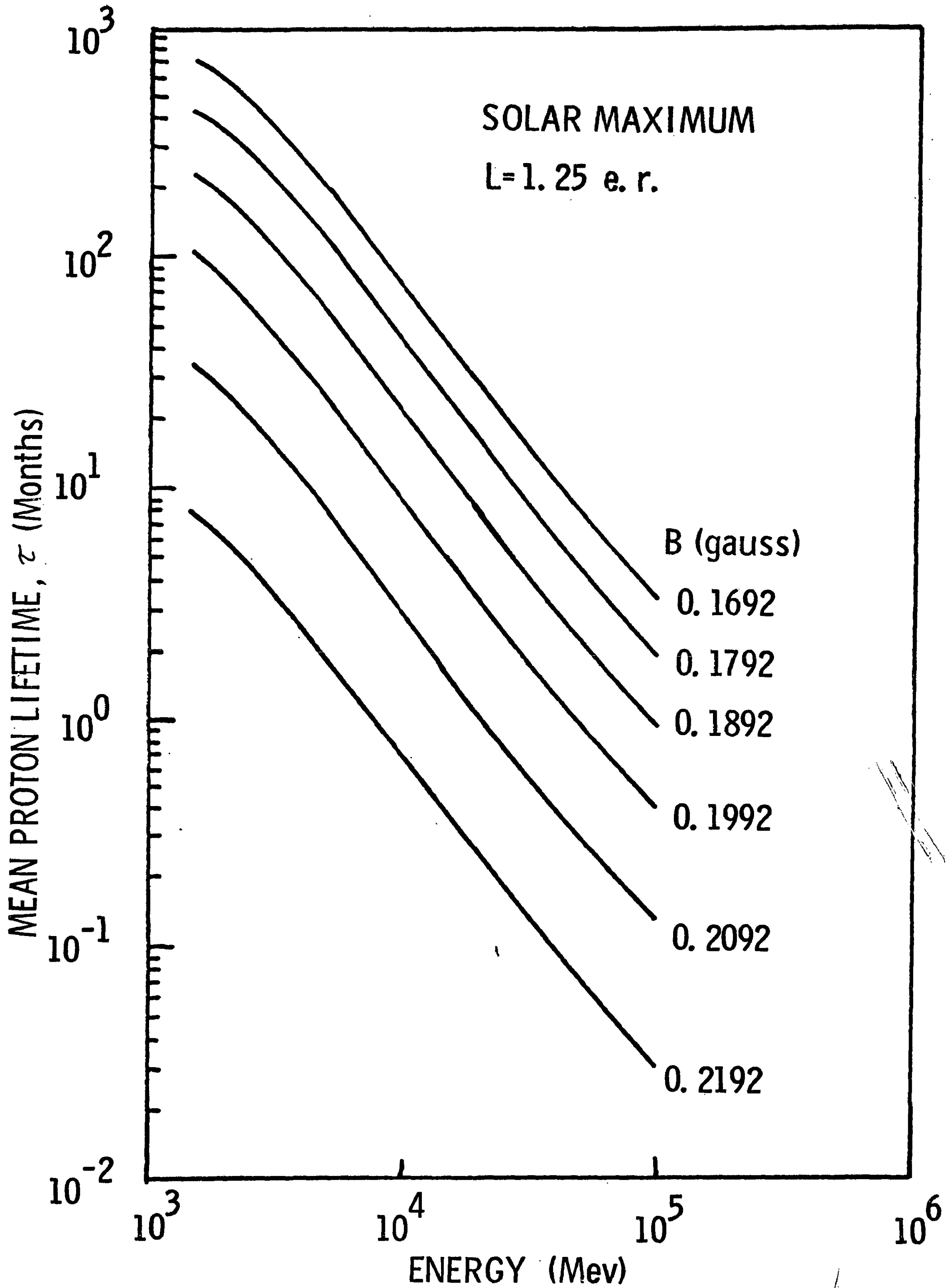

Figure 28. The mean proton lifetime, τ energy spectrum as a function of position at solar maximum.

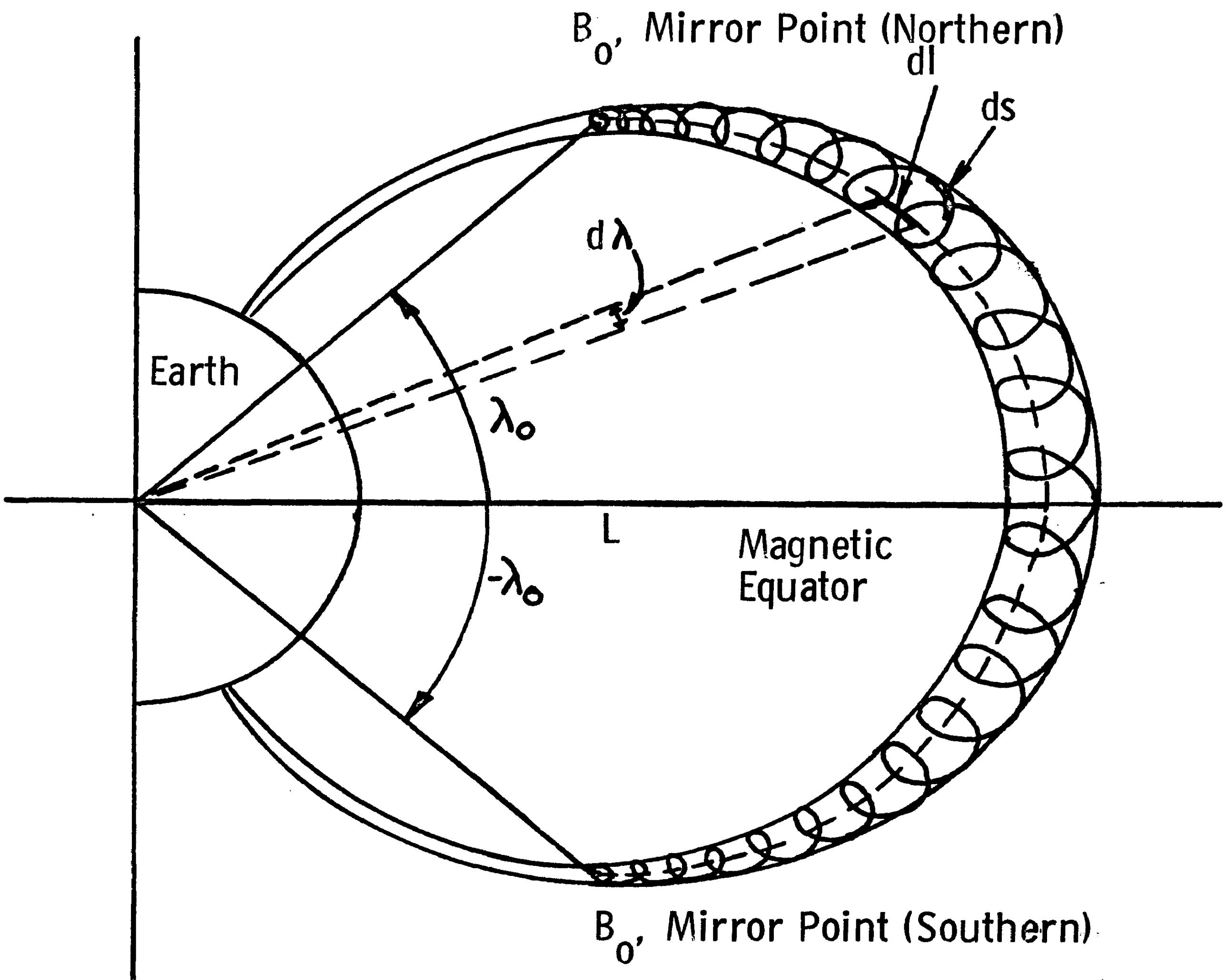

Where:

ds - Element of Arc along the particle's helical trajectory

dl - Element of Arc along the field line

Figure A-I. Schematic of a trapped particle's north-south motion.

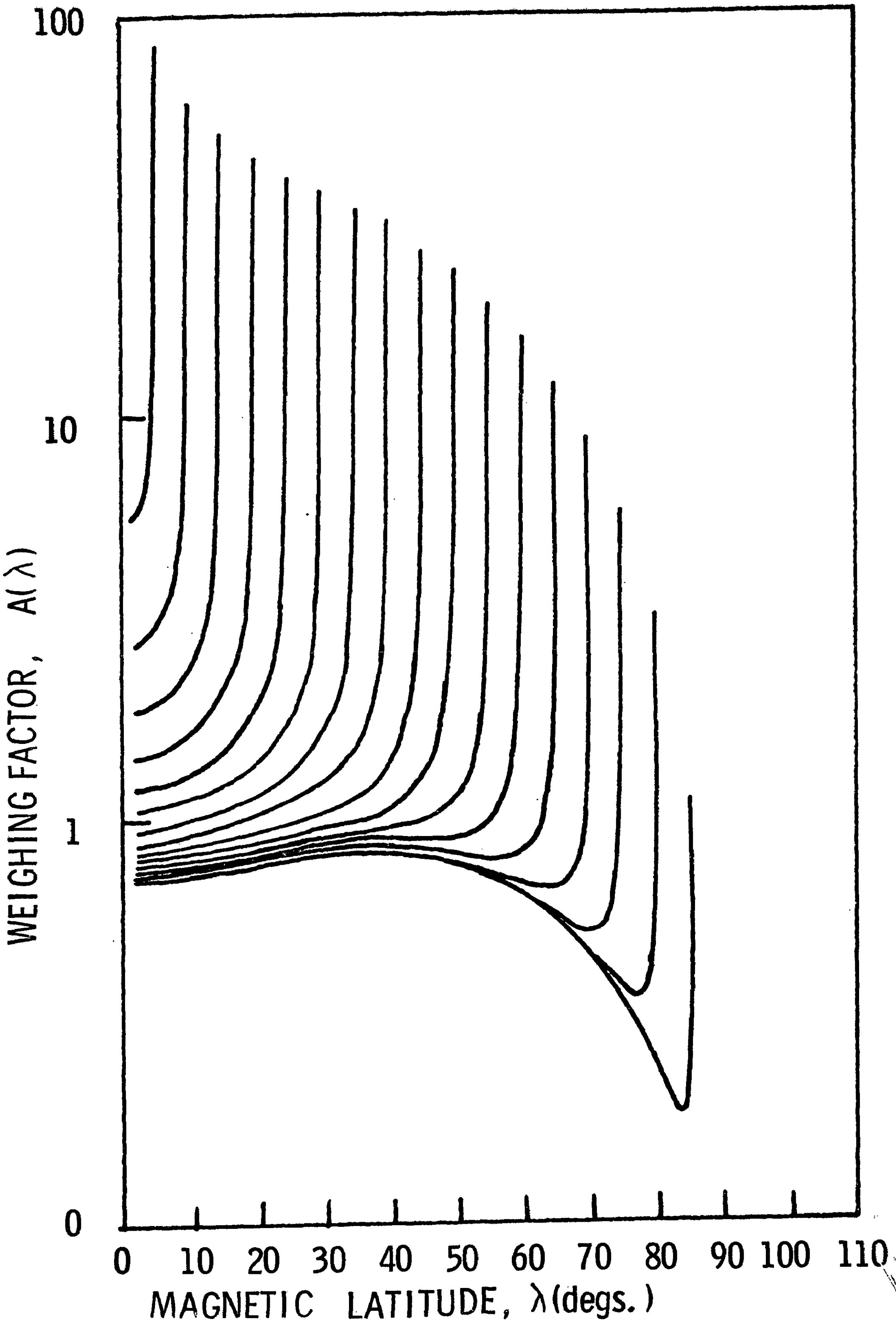

Figure A-II. The weighing factor, A(λ) versus latitude for various mirror latitudes, λ_o, where λ_o are the asympbotes of each curve.

TABLE 1

h(km) \ S	250	200	150	100	70
120	2.500E07	2.500E07	2.500E07	2.500E07	2.500E07
200	4.413E06	4.872E06	5.484E06	6.319E06	6.982E06
300	2.642E06	2.843E06	3.050E06	3.205E06	3.212E06
400	1.945E06	2.007E06	2.012E06	1.885E06	1.689E06
500	1.499E06	1.477E06	1.390E06	1.154E06	9.272E05
600	1.176E06	1.107E06	9.646E05	7.236E05	5.231E05
700	9.327E05	8.387E05	6.842E05	4.607E05	3.021E05
800	7.461E05	6.422E05	4.916E05	3.004E05	1.783E05
900	6.016E05	4.964E05	3.574E05	1.984E05	1.074E05
1000	4.886E05	3.871E05	2.628E05	1.331E05	6.593E04
1100	3.995E05	3.044E05	1.953E05	9.050E04	4.119E04
1200	3.287E05	2.411E05	1.466E05	6.238E04	2.616E04
1300	2.721E05	1.925E05	1.110E05	4.353E04	1.687E04
1400	2.265E05	1.547E05	8.482E04	3.074E04	1.104E04
1500	1.895E05	1.251E05	6.537E04	2.195E04	7.328E03
1600	1.595E05	1.019E05	5.078E04	1.584E04	4.925E03
1700	1.348E05	8.346E04	3.974E04	1.155E04	3.351E03
1800	1.145E05	6.875E04	3.133E04	8.497E03	2.306E03
1900	9.774E04	5.696E04	2.487E04	6.308E03	1.605E03
2000	8.378E04	4.743E04	1.988E04	4.724E03	1.128E04

Diurnal averaged number densities of He as a function of altitude for five solar flux numbers.

TABLE 2

h(km.) \ S	250	200	150	100	70
120	7.600E10	7.600E10	7.600E10	7.600E10	7.600E10
200	3.600E09	3.457E09	3.209E09	2.795E09	2.416E09
300	8.870E08	7.134E08	5.124E08	2.809E08	1.564E08
400	3.054E08	2.054E08	1.112E08	4.025E07	1.471E07
500	1.168E08	6.616E07	2.788E07	6.771E06	1.675E06
600	4.749E07	2.287E07	7.708E06	1.273E06	2.183E05
700	2.024E07	8.364E06	2.232E06	2.611E05	3.153E04
800	8.983E06	3.207E06	6.918E05	5.747E04	4.946E03
900	4.130E06	1.282E06	2.252E05	1.342E04	8.320E02
1000	1.960E06	5.312E05	7.645E04	3.301E03	1.488E02
1100	9.567E05	2.275E05	2.696E04	8.502E02	2.810E01
1200	4.791E05	1.003E05	9.834E03	2.284E02	5.381E00
1300	2.456E05	4.538E04	3.701E03	6.379E01	1.162E00
1400	1.287E05	2.106E04	1.434E03	1.848E01	2.527E-1
1500	6.878E04	9.997E03	5.706E02	5.541E00	5.729E-2
1600	3.746E04	4.849E03	2.330E02	1.717E00	1.352E-2
1700	2.077E04	2.399E03	9.744E01	5.486E-1	3.312E-3
1800	1.170E04	1.210E03	4.170E01	1.806E-1	8.412E-4
1900	6.700E03	6.216E02	1.824E01	6.079E-2	2.212E-4
2000	3.893E03	3.247E02	8.149E00	2.128E-2	6.010E-5

Diurnal averaged number densities of O as a function of altitude for five solar flux numbers.

TABLE 3

h(km.) \ S	250	200	150	100	70
120	1.200E11	1.200E11	1.200E11	1.200E11	1.200E11
200	9.900E08	7.910E08	5.699E08	3.438E08	2.151E08
300	7.683E07	4.269E07	1.791E07	4.503E06	1.188E06
400	1.020E07	4.069E06	1.048E06	1.191E05	1.427E04
500	1.217E06	4.886E05	7.983E04	4.808E03	2.444E02
600	3.142E05	6.758E04	7.106E03	1.857E02	5.155E00
700	6.428E04	1.033E03	7.062E02	9.135E00	1.265E-1
800	1.364E04	1.714E03	7.688E01	5.002E-1	3.528E-3
900	3.242E03	3.031E02	8.962E00	3.010E-2	1.102E-4
1000	7.981E02	5.682E01	1.122E00	1.975E-3	3.821E-6
1100	2.056E02	1.122E01	1.493E-1	1.403E-4	1.459E-7
1200	5.526E01	2.322E00	2.106E-2	1.074E-5	5.274E-9
1300	1.544E01	5.028E-1	3.139E-3	8.835E-7	2.788E-10
1400	4.474E00	1.136E-1	4.927E-4	7.772E-8	1.382E-11
1500	1.342E00	2.778E-2	8.124E-5	7.292E-9	7.412E-13
1600	4.157E-1	6.520E-3	1.405E-5	7.277E-10	4.288E-14
1700	1.328E-1	1.653E-3	2.541E-6	7.702E-11	2.667E-15
1800	4.370E-2	4.342E-4	4.800E-7	8.627E-12	1.777E-16
1900	1.478E-2	1.177E-4	9.452E-8	1.200E-12	1.267E-17
2000	5.142E-3	2.906E-5	1.937E-8	1.270E-13	9.626E-19

Diurnal averaged number densities of O_2 as a function of altitude for five solar flux numbers.

TABLE 4

h(km.) \ S	250	200	150	100	70
120	5. 800E11	5. 800E11	5. 800E11	5. 800E11	5. 800E11
200	7. 393E09	6. 180E09	4. 743E09	3. 136E09	2. 124E09
300	7. 630E08	4. 639E08	2. 210E08	6. 739E07	2. 113E07
400	1. 278E08	5. 777E07	2. 151E07	2. 682E06	4. 225E05
500	2. 562E07	8. 798E06	1. 810E06	1. 407E05	1. 156E04
600	5. 730E06	1. 521E06	3. 239E05	8. 800E03	3. 844E02
700	1. 403E06	2. 884E05	2. 763E04	6. 190E02	1. 471E01
800	3. 664E05	5. 883E04	3. 899E03	4. 802E01	6. 320E-1
900	1. 012E05	1. 276E04	5. 894E02	4. 057E00	3. 006E-2
1000	2. 932E04	2. 918E03	9. 470E01	3. 702E-1	1. 570E-3
1100	8. 862E03	6. 994E02	1. 609E01	3. 627E-2	8. 936E-5
1200	2. 783E03	1. 725E02	2. 878E00	3. 798E-3	1. 016E-5
1300	9. 053E02	4. 558E01	5. 404E-1	4. 237E-4	3. 674E-7
1400	3. 041E02	1. 233E01	1. 063E-1	5. 017E-5	2. 633E-8
1500	1. 075E02	3. 456E00	2. 183E-2	6. 287E-6	2. 023E-9
1600	3. 768E01	1. 002E00	4. 677E-3	8. 321E-7	1. 661E-10
1700	1. 380E01	3. 001E-1	1. 042E-3	1. 160E-7	1. 454E-11
1800	5. 211E00	9. 268E-2	2. 313E-4	1. 699E-8	1. 353E-12
1900	2. 005E00	2. 949E-2	5. 746E-5	2. 612E-9	1. 334E-13
2000	7. 927E-1	9. 654E-3	1. 431E-5	4. 619E-10	1. 393E-14

Diurnal averaged number densities of N_2 as a function of altitude for five solar flux numbers.

TABLE 5

S / h(km.)	250	200	150	100	70
120	4.356E04	4.356E04	4.356E04	4.356E04	4.356E04
200	1.071E04	1.224E04	1.447E04	1.790E04	2.104E04
300	8.035E03	9.323E03	1.114E04	1.380E04	1.611E04
400	7.205E03	8.328E03	9.837E03	1.189E04	1.352E04
500	6.690E03	7.660E03	8.898E03	1.046E04	1.157E04
600	6.272E03	7.102E03	8.107E03	9.263E03	9.974E03
700	5.904E03	6.609E03	7.415E03	8.214E03	8.638E03
800	5.573E03	6.168E03	6.803E03	7.360E03	7.518E03
900	5.272E03	5.769E03	6.260E03	6.597E03	6.571E03
1000	4.996E03	5.408E03	5.774E03	5.933E03	5.768E03
1100	4.742E03	5.079E03	5.339E03	5.352E03	5.083E03
1200	4.502E03	4.778E03	4.947E03	4.843E03	4.495E03
1300	4.291E03	4.503E03	4.594E03	4.395E03	3.989E03
1400	4.090E03	4.250E03	4.275E03	3.998E03	3.552E03
1500	3.903E03	4.018E03	3.986E03	3.647E03	3.173E03
1600	3.730E03	3.804E03	3.723E03	3.335E03	2.843E03
1700	3.568E03	3.606E03	3.484E03	3.057E03	2.555E03
1800	3.417E03	3.424E03	3.266E03	2.809E03	2.303E03
1900	3.276E03	3.255E03	3.066E03	2.587E03	2.081E03
2000	3.144E03	3.098E03	2.884E03	2.387E03	1.886E03

Diurnal averaged number densities of H as a function of altitude for five solar flux numbers.

VITA

ROBERT CHARLES BLANCHARD

Born in Scranton, Pennsylvania, July 16, 1938. Graduated from Scranton Technical High School in that city, June, 1955; B. S. in Physics (cum laude); University of Scranton, 1959. Employed by NASA, Manned Spacecraft Center, Langley Field, Langley Field, Virginia from July, 1959 to February, 1962. The area of work involved trajectory analysis support for Projects Mercury and Apollo. In September, 1960, the author entered William and Mary on a part time basis. February, 1962, the author transferred to present position at NASA, Goddard Space Flight Center, Greenbelt, Maryland. The area of work is applied theoretical studies in the Theoretical Division, dealing primarily with astrodynamics and related topics.